UNIVERSIDADE FEDERAL DE PERNAMBUCO
CENTRO DE CIÊNCIAS DA SAÚDE
DEPARTAMENTO DE CIÊNCIAS FARMACÊUTICAS
PROGRAMA DE PÓS-GRADUAÇÃO EM CIÊNCIAS FARMACÊUTICAS

CLÁUDIO HENRIQUE RODRIGUES DA SILVA

INATIVAÇÃO FOTODINÂMICA DE MICRORGANISMOS RESISTENTES MEDIADA POR AZUL DE METILENO E NANOPRISMAS DE PRATA

RECIFE
2022

CLÁUDIO HENRIQUE RODRIGUES DA SILVA

INATIVAÇÃO FOTODINÂMICA DE MICRORGANISMOS RESISTENTES MEDIADA POR AZUL DE METILENO E NANOPRISMAS DE PRATA

Dissertação apresentada ao Programa de Pós-Graduação em Ciências Farmacêuticas da Universidade Federal de Pernambuco, como requisito parcial para obtenção do título de mestre em Ciências Farmacêuticas.

Área de concentração: Fármacos e medicamentos
Linha de pesquisa: Produção e controle de medicamentos

Orientadora: Profª Drª Beate Saegesser Santos

*Bolsista CAPES

Recife
2022

Catalogação na Fonte
Bibliotecário: Rodriggo Leopoldino Cavalcanti I, CRB4-1855

S586i Silva, Cláudio Henrique Rodrigues da.
Inativação fotodinâmica de microrganismos resistentes mediada por azul de metileno e nanoprismas de prata / Cláudio Henrique Rodrigues da Silva. – 2022.
70 f. : il. ; 30 cm.

Orientadora : Beate Saegesser Santos.
Dissertação (Mestrado) – Universidade Federal de Pernambuco. Centro de Ciências da Saúde. Programa de Pós-Graduação em Ciências Farmacêuticas. Recife, 2022.

Inclui referências e apêndices.

1. Fármacos Fotossensibilizantes. 2. Resistência Microbiana a Medicamentos. 3. Nanopartículas. 4. Fotoquimioterapia. I. Santos, Beate Saegesser (Orientadora). II. Título.

615 CDD (23.ed.) UFPE (CCS2022-283)

CLÁUDIO HENRIQUE RODRIGUES DA SILVA

INATIVAÇÃO FOTODINÂMICA DE MICRORGANISMOS RESISTENTES MEDIADA POR AZUL DE METILENO E NANOPRISMAS DE PRATA

Dissertação apresentada ao Programa de Pós-Graduação em Ciências Farmacêuticas da Universidade Federal de Pernambuco, como requisito parcial para obtenção do título de mestre em Ciências Farmacêuticas.

Área de concentração: Fármacos e medicamentos

Aprovada em: 24/02/2022

BANCA EXAMINADORA

Profª. Drª. Beate Saegesser Santos (Presidente)

Universidade Federal de Pernambuco

Drª Camila Galvão de Andrade (1ª Examinadora)

Universidade Federal de Pernambuco

Dr. Franz de Assis Graciano dos Santos (2º Examinador)

Universidade Federal de Pernambuco

Aos meus pais, com todo amor e gratidão.

AGRADECIMENTOS

A Deus pela vida, oportunidades, sonhos e conquistas.

Aos meus pais, por sempre acreditar e apoiar meus sonhos, por todo o incentivo que deram em toda a minha educação e por todo o carinho e esperança que depositam em mim.

Me agradeço por todos os momentos que pensei em desistir, por todos os momentos em que as coisas ficaram difíceis e eu sempre tentei ver um caminho positivo, sempre tentei procurar coisas boas no meio de tantas adversidades que andam ocorrendo.

A minha orientadora, Profª Drª Beate Santos, meu exemplo de pesquisadora, por ter me dado uma oportunidade de conhecer e me encantar com a nanotecnologia. Não conseguimos nada na vida se as oportunidades não estão lá para que sejam alcançadas. Agradeço muito pelos seis anos que já convivo em seu laboratório, pela grande amizade, por todos os conselhos, ensinamentos e confiança depositada.

A minha co-orientadora, Profª Drª Danielle Macêdo, que abriu as portas do Laboratório de Análises Microbiológicas de braços abertos e topou todos os desafios. Agradeço por todos os ensinamentos e por toda palavra amiga e alegria quando em sua companhia.

A minha grande amiga Bruna Cardoso, que sempre torceu por minhas vitórias e sempre esteve comigo em diferentes momentos da minha vida. Obrigado por ser um porto seguro e por sempre me acompanhar nas caminhadas da vida.

A Joalen Monte, um amigo que a pesquisa me deu e já temos uns bons anos de uma grande amizade, por todo o otimismo e confiança que deposita em mim. Muitas vezes mais do que a que eu mesmo tenho.

A André Bispo, meu companheiro, por todos esses últimos meses. Por sempre me acalmar quando tudo parecia complicado, por acreditar em mim, por todo o carinho, cuidado e torcida em diferentes conquistas e contextos.

Aos meus amigos de profissão com quem dividi preciosos anos da minha vida, Milena Couto, Wilma Oliveira, Júnior Cavalcanti, Débora Nascimento, Alice Carmo, Josenildo Sena, Renata Sobral e Thiago Nascimento. Vocês são profissionais brilhantes, cada um em sua atuação e obrigado por todos os maravilhosos momentos que vivemos desde a época de graduação.

A Marques Leonel, uma pessoa indispensável para a realização desse trabalho, por sempre estar disposto a ajudar, por sempre me ouvir (mesmo quando eu parecia estar sendo muito repetitivo), por ser um ombro amigo quando tudo parecia dar errado, por prover tantas horas de ajuda quando nunca se teve a obrigação.

A João Matheus por todos os momentos vividos no laboratório, na academia, nos caminhos para diferentes locais, por todas as conversas e grande amizade que dividimos. Por sempre estar disposto a me ouvir, como amigo ou como colaborador em seu projeto.

Aos amigos e colegas do Laboratório de Interfaces, Nanomateriais e Sistemas Coloidais, Bruna Pereira, Evanísia Góes, Gricirene Correia, Antônio Gomes, Nayara Cely, Dimitri, Thiago, Júlia. Aos colegas do Laboratório de Análises Microbiológicas, Débora Lopes, Ianca e Mayara. A Thiago Pajeú e equipe do LABTECBIO por toda disponibilidade.

Aos professores que contribuíram diretamente para a realização deste trabalho Goreti Pereira, Adriana Fontes, Ana Porto, Mariane Cajubá, e tantos outros. Meus sinceros agradecimentos.

A Camila Andrade e Franz Santos por aceitar o convite para compor a banca, pela paciência e todas as contribuições ao trabalho.

A Rilvan, secretário da pós graduação, sempre solícito e disposto a ajudar e resolver diferentes problemas enfrentados durante este período.

Ao Programa de Pós Graduação em Ciências Farmacêuticas por todo o apoio e incentivo no desenvolvimento deste trabalho.

A Coordenação de Aperfeiçoamento de Pessoal de Nível Superior pela bolsa de estudos, ao Conselho Nacional de Desenvolvimento Científico e Tecnológico e Fundação de Amparo à Ciência e Tecnologia do Estado de Pernambuco pelo fomento à pesquisa por meio dos projetos vigentes.

“...Though I’m past one hundred thousand miles
I’m feeling very still
And I think my spaceship knows which way to go….”
(BOWIE, 1969, Space Oddity)

RESUMO

As nanopartículas metálicas exibem diversas propriedades que vêm sendo estudadas nos últimos anos em diferentes áreas do conhecimento, principalmente as de prata e ouro. Um efeito característico destas, a ressonância de plásmons de superfície (RPS) confere a capacidade de aumento de propriedades ópticas de outras moléculas, quando em condições específicas. Na área da saúde, uma possibilidade de uso desses sistemas é na associação aos chamados fotossensibilizadores (FS), que são utilizados para a produção de espécies reativas de oxigênio, quando combinados com a luz na Terapia Fotodinâmica, tendo uma modalidade para microrganismos denominada inativação fotodinâmica (IFD). Nesse estudo, nanoprismas de prata foram preparados, caracterizados e posteriormente conjugados com o FS azul de metileno (AM), que tem amplo uso na prática clínica e aprovação pelo órgão regulatório nacional. O objetivo foi aplicar os conjugados na IFD de dois isolados resistentes: *Staphylococcus aureus* isolado da mastite bubalina e *Candida albicans* isolado da balanopostite. Medidas de espectroscopia mostraram que a associação entre os nanoprismas e AM promoveu mudanças de intensidade na fluorescência, de acordo com a concentração do FS empregada, tendo um aumento de *ca* 30% observados para a dose de 100 $\mu mol.L^{-1}$. Foi observado um potencial de superfície (ζ) estável para os nanoprismas (ζ = -51.7 ± 0.55 mV), que reduziu proporcionalmente a concentração de AM (para 25 $\mu mol.L^{-1}$, ζ = -43.36 ± 0.37mV e para 100 $\mu mol.L^{-1}$, -3.40 ± 0.15 mV). A ausência de toxicidade dos sistemas coloidais obtidos foi determinada frente a linhagem de macrófagos sadios. Os ensaios de IFD utilizando uma fonte de luz vermelha (45.87 $mW.cm^{-2}$) com tempos de 3, 6 e 9 minutos mostraram que, no menor tempo, obteve-se total inativação do inóculo, numa [AM] = 45 $\mu mol.L^{-1}$. Para a total inativação de *C. albicans* precisou-se irradiar 2 min, para o conjugado contendo [AM] = 100 $\mu mol.L^{-1}$. Em todos os cenários testados, o AM não demonstrou inativação fotodinâmica total. Os resultados evidenciam a capacidade dos conjugados como eficientes fotossensibilizadores para posteriores aplicações *in vivo*, inclusive em patologias que há relato de resistência.

Palavras-chave: agentes fotossensibilizantes; resistência microbiana a medicamentos; nanopartículas; fotoquimioterapia

ABSTRACT

Metallic nanoparticles exhibit several properties that have been studied in recent years in different areas of knowledge, especially those of silver and gold. A characteristic effect is surface plasmon resonance (SPR), that confers the ability to increase optical properties of other molecules under specific conditions. In the health area, one possibility of using these systems is in association with the so-called photosensitizers (PS), which are used for the production of reactive oxygen species, when combined with light in Photodynamic Therapy, having a modality for microorganisms called photodynamic inactivation. (PDI). In this study, silver nanoprisms were prepared, characterized and subsequently conjugated with PS methylene blue (MB), which has wide use in clinical practice and has been approved by the national regulatory agency. The objective was to apply the conjugates in the PDI of two resistant isolates: Staphylococcus aureus isolated from buffalo mastitis and Candida albicans isolated from balanoposthitis. Spectroscopy measurements showed that the association between nanoprisms and MB promoted changes in fluorescence intensity, according to the concentration of PS used, with an increase of *ca* 30% observed for the dose of 100 µmol.L^{-1}. A stable surface potential (ζ) was observed for nanoprisms (ζ = -51.7 ± 0.55 mV), which proportionally reduced in the presence of MB (for 25 µmol.L^{-1}, ζ = -43.36 ± 0.37mV and for 100 µmol.L^{-1}, -3.40 ± 0.15 mV). The absence of toxicity of colloidal systems obtained was determined against the lineage of healthy macrophages. PDI assays showed that the time required for total inactivation of the S. aureus strain was 3 min with the conjugate (for [MB] = 45 µmol. L^{-1} in the conjugate). For total inactivation of C. albicans, it was necessary to irradiate 2 min for the conjugate containing [MB] = 100 µmol.L^{-1}. In both experiments and under the same conditions, MB did not show total photodynamic inactivation. The results show the ability of the conjugates as efficient photosensitizers for later in vivo applications, including in pathologies where resistance is reported.

Keywords: photosensitizers agents; Microbial drug resistance; nanoparticles; photoquimiotherapy

LISTA DE ABREVIATURAS E SIGLAS

AgNPs	Nanopartículas de prata
AM	Azul de metileno
ATCC	*American Type Culture Collection*
EROs	Espécies reativas de oxigênio
FS	Fotossensibilizadores
IFD	Inativação fotodinâmica
MEV	Microscopia eletrônica de varredura
MET	Microscopia eletrônica de transmissão
RPS	Ressonância de plásmons de superfície
RNO	*N,N*-dimetil-4-nitrosanilina
TFD	Terapia fotodinâmica
TFDa	Terapia fotodinâmica antimicrobiana
UV-Vis	Ultravioleta-Visível

LISTA DE SÍMBOLOS

nm	nanômetros
Ag^{+}	íon prata
e^{-}	elétrons
O_2	oxigênio molecular
O_2^{-}	ânion superóxido
H_2O_2	peróxido de hidrogênio
OH^{-}	radical hidroxila
pH	potencial hidrogeniônico
$^1O_2$	oxigênio singleto
$^3O_2$	oxigênio tripleto
%	percentagem
PO_4^{3-}	íon ortofosfato
µm	micrômetro
g	grama

SUMÁRIO

1 INTRODUÇÃO

O aumento da resistência dos microrganismos aos tratamentos convencionais tem compelido a busca de formas alternativas mais eficientes de tratamento. Neste sentido, a Terapia Fotodinâmica (TFD), que consiste basicamente no emprego de uma luz de baixa potência com uma molécula fotossensível para gerar espécies reativas de oxigênio, vem emergindo nas últimas décadas. Entre as luzes utilizadas, temos lasers e LEDs para a ativação dos chamados agentes fotossensibilizadores (FS), que quando irradiados na região da luz visível, reagem com o oxigênio e geram espécies reativas de oxigênio (EROs), levando à morte celular no alvo de atuação.

Diversas aplicações já são relatadas para a TFD, como na oncologia, dermatologia e odontologia. Quando voltada para a inativação de microrganismos, temos uma modalidade denominada Inativação Fotodinâmica (IFD), que é amplamente estudada para aplicação frente aos microrganismos que vem adquirindo resistência ao longo dos anos.

Diversas moléculas podem ser utilizadas como FS e, entre elas, podemos destacar moléculas das classes de fenotiazinas (p.ex, Azul de Metileno, AM). O AM é um fotossensibilizador de amplo uso, por conta de seu baixo custo em comparação a outras classes e também possui a vantagem de já ser aprovado por diferentes órgãos reguladores. Um dos exemplos de seu uso é na forma de solução para o tratamento de periodontite bacteriana (SGOLASTRA et al., 2013).

Visando melhoria na eficácia dos FS, bem como a melhoria de parâmetros da TFD, que se relacionam diretamente com características destes, novas propostas vêm surgindo baseadas no uso da nanotecnologia. Entre essas, temos a encapsulação de moléculas fotossensíveis em nanopartículas poliméricas, e também recursos no campo da plasmônica, por meio da transferência de energia de nanopartículas, como as nanopartículas de prata.

Uma das principais características das AgNPs é a ressonância de plásmons de superfície que permite a interação entre a radiação eletromagnética incidente e os elétrons das bandas de condução nos nanometais. Tais processos conduzem a efeitos de campos ópticos próximos a tais nanoestruturas, culminando em fenômenos de amplificação do sinal original, como por exemplo, os que envolvem processos de emissão de luz.

Este efeito depende da morfologia das partículas no meio coloidal, as quais podem ser obtidas na forma de: esferas, bastões, prismas e estruturas complexas como estrelas (GÓMEZ *et al*, 2018), e que possui diversas aplicações, como catalíticas, ópticas, biomédicas, farmacêuticas e no desenvolvimento de sensores (FAIRUZI *et al*, 2018). Além disso, também há um amplo campo de utilização na amplificação de fluorescência através de efeitos plasmônicos, com aplicações no combate bacteriano através da Terapia Fotodinâmica (MELO *et al*, 2012). Por outro lado, AgNPs já vem sendo aplicadas na área biomédica como agentes antibacterianos, principalmente no intuito de proteger superfícies frente ao crescimento de biofilmes bacterianos por meio de mecanismos de redução de adesão bacteriana (FREIRE *et al*, 2018).

Uma das interações que decorrem da associação entre um fotossensibilizador e uma nanopartícula é a transferência de energia. Esse efeito é dependente de algumas condições, como a distância, em nanômetros, do máximo de absorção e de extinção destes. Quando próximos, por conta do efeito de ressonância de plásmons de superfície, que é uma característica bastante estudada das partículas, podemos ter a concentração de elétrons num determinado lado da partícula e a transferência para o fotossensibilizador no estado excitado tripleto. Essa doação faz com que a geração de espécies reativas seja mais eficaz, e com isso, uma melhora na atividade fotodinâmica é observada.

Devido ao aumento da resistência microbiana, diferentes formas de tratamento que venham atuar como complementares são comumente estudadas. Por esta razão, este trabalho estudou o efeito da inativação fotodinâmica com conjugados provenientes da associação de nanoprismas de prata com o azul de metileno frente a uma cepa de *Staphylococcus aureus* isolado da mastite bubalina. Outro microrganismo estudado foi a *Candida albicans*, que foi isolada de um indivíduo acometido com balanopostite, resistente ao tratamento com azóis

2 OBJETIVOS

2.1 OBJETIVO GERAL

Desenvolver sistemas nanoestruturados conjugados em meio coloidal, entre nanoprismas de prata com azul de metileno e avaliar seu potencial uso na inativação fotodinâmica de microrganismos resistentes isolados de patologias.

2.2 OBJETIVOS ESPECÍFICOS

I. Preparar nanoprismas de prata utilizando a metodologia de crescimento por semente;
II. Conjugar eletrostaticamente o azul de metileno e nanoprismas de prata;
III. Caracterizar os sistemas obtidos, através de diferentes metodologias analíticas (morfológicas, espectroscópicas e coloidais);
IV. Avaliar a eficácia de produção de espécies reativas utilizando a detecção indireta pela degradação da N,N-dimetil-3,4-nitrosanilina;
V. Utilizar a metodologia de inativação fotodinâmica frente a isolados de *Staphylococcus aureus* e *Candida albicans* com perfil de resistência.

3 REFERENCIAL TEÓRICO

3.1 MICRORGANISMOS E RESISTÊNCIA

O uso não racional de antimicrobianos tem sido uma preocupação para os profissionais de saúde e indústrias farmacêuticas. Com a com descoberta da penicilina, em 1928, teve início Era dos Antibióticos. O uso indiscriminado de antimicrobianos por parte de prescritores, da população que pratica a automedicação e também no setor agropecuário levou ao desenvolvimento de superresistência as terapias convencionais, fazendo necessário o desenvolvimento de antimicrobianos cada vez mais potentes e de espectro aumentado, elevando assim os custos do processo de fabricação e trazendo também o custo de vidas que se perdem decorrente de infecções por superbactérias não responsivas aos tratamentos convencionais (BUSH *et al.*, 2011; DODDS, 2017).

Mesmo com a sofisticação tecnológica que temos alguns microrganismos são capazes de desenvolverem mecanismos ainda mais eficazes que transpõem as nossas tecnologias e não sabemos até que ponto seremos eficientes em desenvolver fármacos capazes de se sobressaírem a esses microrganismos super-resistentes (SILVA; AQUINO, 2018). Deve-se considerar também os altos custos no desenvolvimento e a pequena perspectiva de retorno financeiro por parte das indústrias farmacêuticas (DODDS, 2017).

Diante do exposto fica clara a inadiável necessidade de desenvolvimento de tecnologias outras que não se utilizem dos antimicrobianos convencionais. É a partir dessa perspectiva que novas áreas como a área da fotônica, especificamente a biofotônica (utilização de luz e instrumentos da óptica em questões que se relacionem com os seres vivos) e mais diretamente a terapia fotodinâmica, podem trazer novos horizontes aos problemas já conhecidos.

3.1.1 Mastite

A mastite pode ser definida como uma inflamação aguda das glândulas mamárias, que acomete atualmente uma gama de mamíferos. É uma patologia que pode ser fatal (caso ocorra uma sepse), e tem uma grande relação com a economia, sendo uma das principais causas da redução de produção do leite, mudanças em sua composição e qualidade (GOMES; HENRIQUES, 2016). Além disso, está relacionada diretamente com o bem-estar animal e a segurança alimentar. Uma das principais

preocupações de indústrias de laticínios é a resistência bacteriana que têm aumentado potencialmente nos últimos anos, fazendo com que os antibióticos estejam susceptíveis ou ineficaz o tratamento (HEIKKILÄ *et al.*, 2018).

Entre os principais animais acometidos temos o rebanho de bovinos (SREDNIK *et al.*, 2018), caprinos (HOEKSTRA *et al.*, 2019) e bubalinos (SREDNIK *et al.*, 2018). O principal microrganismo associado a essas infecções é o *Staphylococcus aureus*, além dele, outros patógenos que fazem parte da microbiota também podem estar envolvidos na infecção, como *Streptococcus uberis*, *Escherichia coli*, e *Klebsiella spp* (RUEGG, 2017).

O Brasil, segundo dados do Ministério da Agricultura e pecuária de 2018, possuí o maior rebanho de búfalos do ocidente, sendo quatro raças espalhadas pelo país, principalmente na região Amazônica. Os búfalos se destacam por apresentar uma qualidade nutricional de leite bastante elevada, que contém teores de macromoléculas mais abundantes do que o rebanho bovino, por exemplo. Os mesmos problemas apresentados para os rebanhos bovinos são vistos para os bubalinos quando são acometidos por mastite, que são majoritariamente a queda da qualidade do leite e os altos custos de antibioticoterapia e prevenção (MEDEIROS *et al.*, 2013).

Diversos tratamentos podem ser propostos para a mastite bubalina, uma vez que há uma baixa eficácia no tratamento com antibióticos, que possui um alto custo (SILVA *et al.*, 2016). Entre as alternativas para o tratamento, temos as AgNPs, onde há relatos de inativação de cepas de mastite bovina subclínica (HABIBIAN DEHKORDI; HOSSEINPOUR; KAHRIZANGI, 2011), bem como inativação através de FS, por meio da terapia fotodinâmica frente aos mesmos tipos de microrganismos (MOREIRA *et al.*, 2018). Não existem relatos do uso de AgNPs combinadas a um FS para a inativação fotodinâmica de bactérias isoladas de qualquer rebanho acometido por mastite.

3.1.2 Infecções fúngicas

Fungos são seres dispersos no meio ambiente, em vegetais, ar atmosférico, solo e água, sendo capazes de colonizar o homem e animais e, frente à perda do equilíbrio parasita-hospedeiro podem causar diversos quadros infecciosos, com formas clínicas localizadas ou disseminadas (KAUFFMAN, 2009). As leveduras do gênero *Candida* despertam o interesse médico devido a sua elevada frequência de

colonizar e infectar o ser humano, causando infecções do tipo candidíase, candidoses ou monilíase com amplo espectro clínico (BEN-AMI, 2018).

Fazem parte da microbiota humana e são extremamente oportunistas, adaptáveis e capazes de causar infecções no hospedeiro (DJORDJEVIC *et al.*, 2015). Para que ocorra infecção, ou seja, a mudança de comensal para patogênico, é preciso que ocorra perturbação nas condições, como mudança de clima ou depressão imunológica, acarretando infecções que podem se manifestar de forma cutânea ou até generalizada (KAUFFMAN, 2009). *Candida albicans* é tida como a espécie mais patogênica, sendo o agente etiológico responsável por diferentes infecções clínicas, que vão desde comprometimento superficial em mucosa até infecções sistêmicas com maior grau de severidade (BERTOLINI *et al.*, 2019).

A mudança da morfologia de levedura para hifa é um fator importante para a patogênese, pois causa danos aos epitélios e também induz o processo inflamatório (CLEARY *et al.*, 2016). Outra característica a ser apontada da determinada espécie é a capacidade de adesão a vários sítios anatômicos formando comunidades microbianas chamadas de biofilmes (WALL *et al.*, 2019), que comumente se associam a outros microrganismos, como bactérias (p. ex, *S. aureus* e *Pseudomonas aeruginosa*) e agravam a patologia e o tratamento (LOHSE *et al.*, 2018). Cerca de 30% das mulheres apresentam colonização vaginal, e os casos de infecções fúngicas hospitalares associados a *Candida,* ultrapassam a marca de 70%, o que eventualmente vem restringindo às opções terapêuticas (DADAR *et al.*, 2018).

Candidíase é a denominação dada a infecção derivada de leveduras do gênero *Candida*, onde determinadas espécies são comensais na microbiota da pele e mucosas, podendo acometer órgãos, tecidos e desenvolver diversos quadros clínicos (PRASAD; NAIR; BANERJEE, 2019). As infecções têm emergido com bastante frequência nos últimos anos se tornando um problema grave na saúde pública, afetando principalmente pacientes imunossuprimidos e pacientes internados na UTI (GAJDÁCS *et al.*, 2019). A candidíase pode ocorrer de forma endógena ou exógena, onde ambas se associam com modificações fisiológicas que deriva da imunossupressão. Isso deixa o paciente exposto a diversos riscos, principalmente aqueles acometidos com patologias sistêmicas, que fazem uso de fármacos com alto grau de imunossupressão, bem como o uso prolongado de antibióticos, que modificam

a microbiota e estimulam a disseminação de *Candida* (PINHATI, 2015). De acordo com a clínica apresentada, pode ser classificada em: infecções mucocutâneas (acometem a cavidade oral e órgãos genitais), as infecções cutâneas que são limitadas a pele e anexos, a candidíase invasiva que pode atingir órgãos como bexiga, pulmão coração, entre outros, e a que alcança o sistema sanguíneo, conhecida como infecção sistêmica, responsável por causar a candidemia que pode provocar quadro de septicemia fatal, levando a taxas altas de morbimortalidade (BEN-AMI, 2018).

As classes terapêuticas disponíveis atualmente para o tratamento dessas infecções são os polienos, azólicos e equinocandinas, sendo usados de forma única ou associados na farmacoterapia do paciente. Mas, a ineficácia do tratamento não se limita apenas a resistência e a pouca variedade de fármacos, também é causa pela toxicidade elevada como efeitos adversos sistêmicos que alguns antifúngicos apresentam, por exemplo, nefrotoxicidade (LEE *et al.*, 2021).

Por isso, de acordo com o cenário que vem se desenvolvendo, há um grande interesse no desenvolvimento de novas alterativas terapêuticas, que estejam associadas ao tratamento convencional. A TFD surge como um método alternativo para o tratamento complementar de infecções causadas por *Candida*, principalmente em mucosas e pele.

3.1.2.1 Balanopostite

A balanopostite corresponde a uma infecção que ocorre na glande peniana, tendo como principal público acometido os homens que não são circuncisados. Além desse fator, a imunossupressão, que pode ser causada por outras patologias, como diabetes e AIDS (LISBOA *et al.*, 2010).

O principal microrganismo associado é *Candida albicans*, tendo também relatos de infecções por outros fungos, como *Aspergillus spp.*, alguns dermatófitos e algumas bactérias, a exemplo de *Staphylococcus spp*. e alguns *Streptococcus* do grupo B e D (HU, Yongxuan *et al.*, 2017). *C. albicans* é responsável por *ca* 30-35% de todas as infecções associadas a balanopostite (JEGADISH *et al.*, 2021). A Figura 1 mostra a imagem de um pênis acometido, com a glande comprometida e colonizado por *C. albicans*, que é confirmado com os testes também mostrados.

A resistência de *C. albicans* ao tratamento convencional com azóis já foi relatada na literatura, por meio de um estudo de caso (HU *et al.*, 2017). Visto isso, a TFD pode ser uma ótima alternativa para complementar o tratamento, inclusive com os estudos que envolvem o desenvolvimento de fotossensibilizadores com uma maior eficácia, associando o uso de alguns recursos, como a nanotecnologia.

Figura 1 - Balanopostite causada por *C. albicans,* infeccionando o pênis e gerando fissuras na glande(a), teste com KOH mostrando a presença de pseudohifas e esporos (b), pseudohifas e esporos corados com azul de metileno (c) e crescimento da cultura de C. albicans (d).

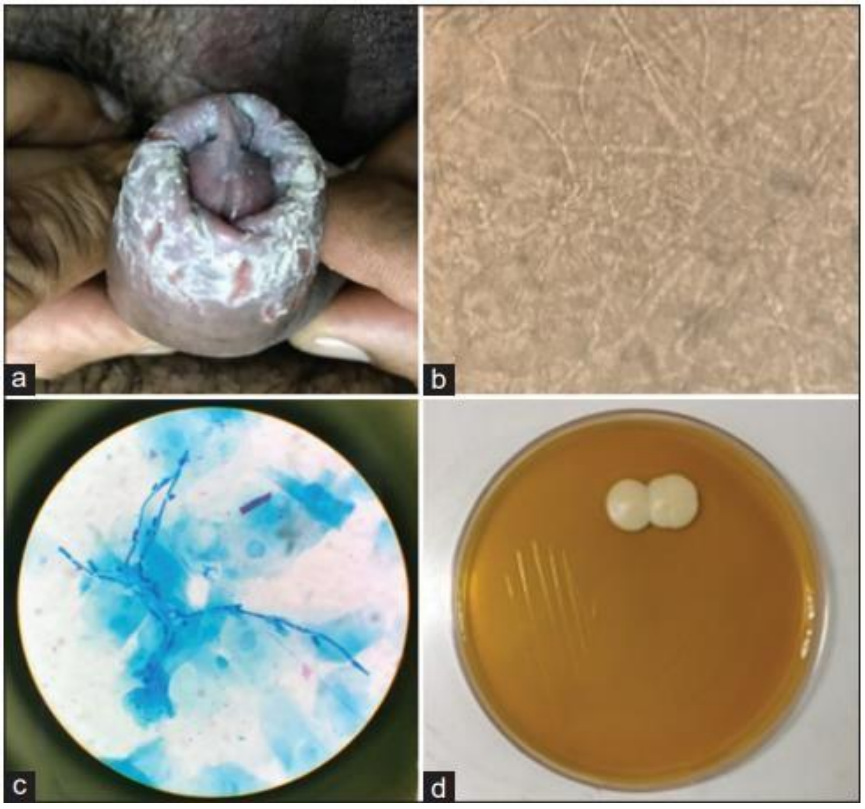

Fonte: Jegadish (2017).

3.2 TERAPIA FOTODINÂMICA

De acordo com Cieplik e colaboradores (2018), a terapia fotodinâmica (TFD) foi descoberta por acidente em 1900, através de estudos de toxicidade do corante vermelho de acridina em *Paramecium spp.*, por Oscar Raab, durante os estudos relacionados a sua tese de doutorado. Inicialmente, foi realizado um estudo com baixas doses que não se mostrou reprodutível, porém, observou-se que alguns parâmetros experimentais influenciavam diretamente nos resultados. Esses parâmetros eram o horário do dia e a quantidade de luz solar que incidia sobre a

amostra. Posteriormente, Hermann von Tappeiner, orientador do Raab, publicou o primeiro estudo sobre inativação de bactérias utilizando a técnica, ainda então chamada de “Fenômeno fotodinâmico”, em 1905 (CIEPLIK *et al.*, 2018). Os principais eventos relacionados ao desenvolvimento da terapia fotodinâmica desde a descoberta até os dias atuais podem ser vistos na Figura 2.

Na TFD, vamos ter a interação simultânea de fotossensibilizadores (FS), luz e oxigênio molecular existente nas células. Para fins diagnósticos, os fotossensibilizadores podem ser empregados como marcadores fluorescentes, já que possuem uma preferência por células cancerosas (BERG *et al.*, 2005). A Figura 3 apresenta um esquema geral que ilustra os diferentes processos que ocorrem a partir da excitação de um fotossensibilizador por uma fonte de luz. A absorção de um fóton de luz promove a excitação e transição do FS do estado fundamental para o estado excitado singleto. Neste estado, ele pode regressar ao estado fundamental por emissão de fluorescência ou passar ao estado excitado tripleto, onde pode reagir com o oxigênio molecular de duas formas: indiretas (reação tipo I e reação tipo II) e diretas (reação tipo III e reação tipo IV) (GARCIA-DIAZ; HUANG; HAMBLIN, 2016; SILVESTRE *et al.*, 2021).

Figura 2 - Histórico da terapia fotodinâmica desde o descobrimento do “fenômeno fotodinâmico” até a aprovação das técnicas utilizadas até os dias

atuais.

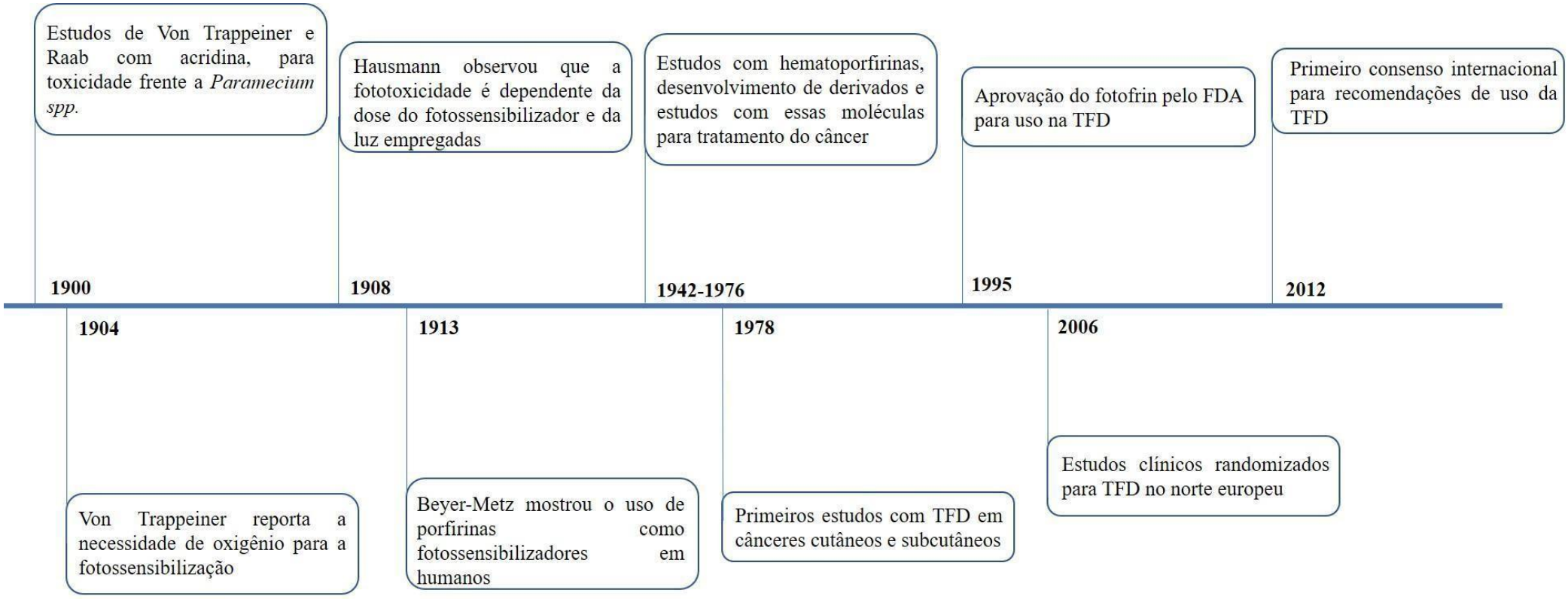

Fonte: O autor, 2021.

Na reação do tipo I, o FS reage diretamente com o substrato, membrana celular ou uma molécula, essa reação permite a transferência de elétrons (e^-) formando íons ou radicais derivados do FS e do substrato (COSTA, 2013). As espécies reativas são formadas por reduções de um ou mais elétrons no oxigênio (O_2). Os produtos desta redução incluem ânion superóxido (O_2^-), peróxido de hidrogênio (H_2O_2), radical alcoxila, radical peroxila e radical hidroxila (OH^-) (ITRI; UCHOA; BAPTISTA, 2013; VIANA, 2015). A reação do tipo II envolve a perda de energia através da emissão de fluorescência (processo radiativo) transferindo esta energia através de um processo de cruzamento intersistemas para o oxigênio molecular, que passa do estado fundamental tripleto para o singleto, o qual possui citotoxicidade intrínseca (PAOLI *et al.*, 2006).

Figura 3 - Esquema ilustrando os possíveis processos durante a terapia fotodinâmica com o processode excitação do FS e formação de ROS após combinação com o oxigênio molecular.

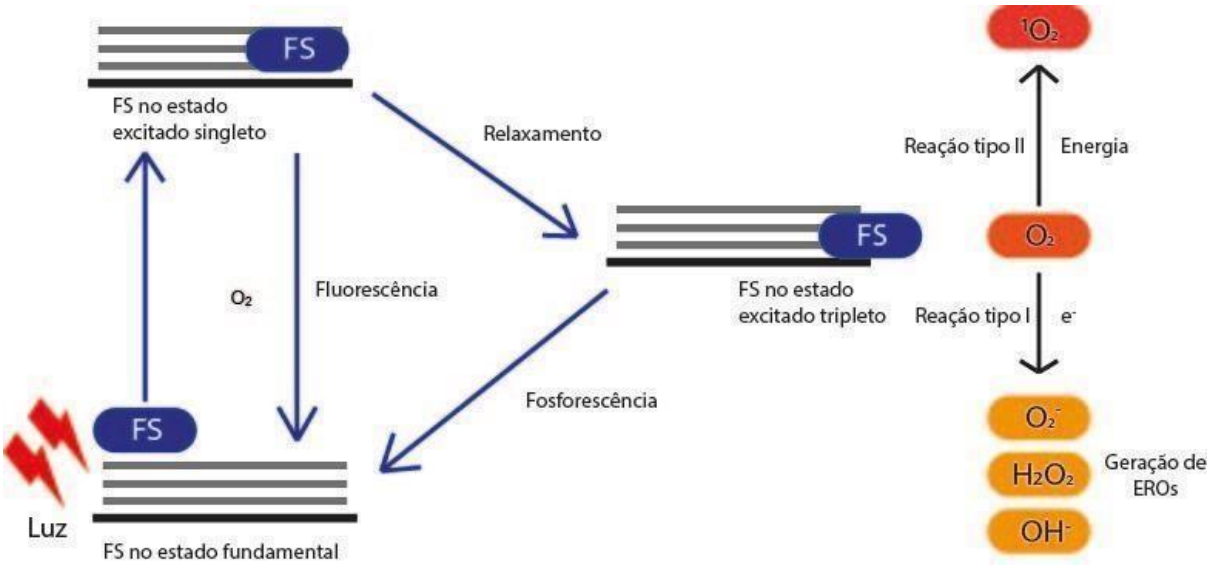

Fonte: Adaptado de VIANA (2015).

Além das reações descritas na Figura 3, temos também as reações III e IV, que são denominadas diretas não necessitarem do oxigênio. Na III, estão envolvidos o FS na sua forma excitada tripleto, oriundo do cruzamento intersistemas, e as espécies reativas já nativas do organismo, que são recrutadas para o local de ação. Na segunda, temos a fotoisomerização do FS na parede da célula quando ele se encontra no estado excitado singleto, através de algumas mudanças estruturais (SILVESTRE *et al.*, 2021).

3.2.1 Inativação fotodinâmica

Atualmente, a TFD vem sendo utilizada como uma estratégia para aniquilar cepas bacterianas resistentes, numa modalidade conhecida como inativação fotodinâmica (IFD). A aplicação da IFD tem como alvo principal o tratamento de infecções localizadas superficiais, como as que ocorrem na pele e cavidade oral, mostrando bons resultados contra uma ampla faixa de microrganismos resistentes a antibióticos (ITRI; UCHOA; BAPTISTA, 2013; VIANA, 2015), tornando-se uma alternativa menos invasiva e mais promissora para erradicação dos microrganismos (GONZÁLEZ-DELGADO *et al.*, 2016).

A terapia fotodinâmica antimicrobiana pode ser uma alternativa interessante na redução microbiana e consequentemente, importante na prevenção e tratamento das lesões cariosas, infecções por bactérias e leveduras. Sendo assim, contribuições teórico-práticas nesta linha de pesquisa são importantes, não só para aumentar o acervo de conhecimentos científicos, mas também para fornecer respaldo científico à democratização do acesso aos usuários da terapia com laser (BAPTISTA *et al.*, 2011).

3.2.2 Fotossensibilizadores

Os fotossensibilizadores são um dos componentes principais para o sucesso da TFD. Para que um FS seja classificado como eficiente, alguns parâmetros devem ser observados, a exemplo sua acumulação seletiva no alvo de ação, boa quantidade de geração de espécies reativas de oxigênio, baixa ou nenhuma atividade na presença da luz, rápida eliminação e caráter anfifílico (CORREIA *et al.*, 2021). Vários compostos vêm sendo testados como FS e utilizados comercialmente, segundo a literatura. Dentre as diversas moléculas utilizadas na TFD, temos a classe das porfirinas, os fenotiazínicos, as clorinas e outras moléculas derivadas de produtos naturais, como a curcumina (PHAM *et al.*, 2021).

Dentre o grupo dos fenotiazídicos, temos o azul de metileno (AM) (Figura 4), um corante catiônico e relativamente lipofílico, que confere a capacidade de permear membranas, e por possuir carga positiva, é atraído pelo potencial negativo das mitocôndrias, tendo uma grande afinidade por esta organela. P(ALVARENGA, Letícia Heineck *et al.*, 2015). É aprovado para uso por diferentes agências reguladoras, como a Food and Drugs Administration (FDA) e também a Agência Nacional de Vigilância Sanitária (ANVISA), tendo com uma dose tóxica estimada em 3.292 $\mu mol.L^{-1}$. Este FS é atualmente empregado no tratamento de infecções bucais, periodontite e

descontaminação endodôntica, bem como em procedimentos de podologia, sendo relatada uma produção de $^1O_2$ em torno de 50% em lasers de uso convencional (ITRI; UCHOA; BAPTISTA, 2013).

Figura 4 - Estrutura molecular do Azul de Metileno.

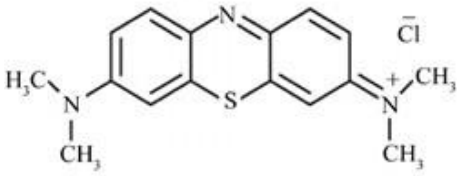

Fonte: Adaptado de Santos (2016).

A literatura já relata o uso do AM para inativação de bactérias (LEAL *et al.*, 2017; SEBRÃO *et al.*, 2016), fungos (ALBERDI; GÓMEZ, 2020; SPEZZIA-MAZZOCCO *et al.*, 2016) e parasitas (CABRAL *et al.*, 2020; PINTO *et al.*, 2017). Também já se relata o uso desse FS para a inativação de biofilmes bacterianos, seja como fotossensibilizador principal da terapia (NEMEZIO *et al.*, 2017), ou em associação com moléculas que desempenham papéis importantes na TFD, como a eritrosina (TOKUBO *et al.*, 2018) e o peróxido de hidrogênio (YANG *et al.*, 2019).

Para melhorar a eficácia do AM, diferentes estratégias já foram utilizadas e são relatadas na literatura. Quanto ao uso de nanopartículas para a melhoria do efeito fotodinâmico, Jesus *et al*, (2018) combinaram AgNPs e AuNPs para inativação de linhagem de câncer de mama (MDA-MB-468) e também estudou a produção de EROs dos sistemas, observando que, o somatório de efeitos promoveu uma maior inativação dos sistemas. Outro relato foi realizado por Parasuraman et al, (2020), que utilizou de conjugados também de AgNPs com o AM para inativação de *S. aureus* e *P. aeruginosa*, e também se verificou que a associação promoveu o aumento do efeito comparado com o FS livre. Entretanto, em nenhum dos relatos, a banda de plásmon do fotossensibilizador estava diretamente próxima ao máximo de absorção do AM, estudo que só aconteceu em 2021, através de um dos capítulos desta dissertação.

3.3 NANOPARTÍCULAS METÁLICAS

A redução dos metais a uma escala nano, correspondente a bilionésima parte do metro ($1x10^{-9}$), os caracterizam em diversas propriedades não vistas no cristal macroscópico, como baixos pontos de fusão, elevada razão área superficial/volume e

inúmeras propriedades ópticas, que se relacionam diretamente com o tamanho e forma das partículas. Comumente, as nanopartículas de prata (AgNPs) apresentam dimensões compreendidas entre 10 e 100 nm, podendo assumir diferentes formas dependendo da metodologia empregada (ZHANG; ERKEY, 2006).

O uso de materiais metálicos na escala nano, e particularmente, a prata, não é uma prática recente. A literatura já relata o uso de AgNPs na antiguidade, como na taça de Lycurgo (BARBER; FREESTONE, 2007) e na adição de cores características a vitrais de catedrais. Há uma grande relação dessas aplicações e as AgNPs, pois a coloração varia de acordo com o fenômeno de modificação do tamanho da partícula. Além das utilizações citadas, elas também têm amplo uso no campo medicinal, devido a propriedades antimicrobianas e antissépticas (QAZI; JAVAID, 2016). O fato de possuir tamanho próximo ao de células e genes, faz com que se tenha um grande interesse de aproximar os nanomateriais e esses sistemas biológicos. Entre as propriedades exibidas pelas AgNPs, a maioria se fundamenta na óptica, por meio de um fenômeno denominado ressonância localizada de plásmons de superfície (RPS), que eleva suas aplicações da fotônica até a área biomédica. Diversos relatos na literatura já mostram o uso de AgNPs como catalisador na degradação de tinturas orgânicas (VIDHU; PHILIP, 2014), agente bacteriano (FRANCI *et al.*, 2015) e amplificador plasmônico (MELO *et al.*, 2012; RIBEIRO *et al.*, 2018).

As propriedades únicas observadas para as AgNPs variam de acordo com a sua morfologia. Diversas metodologias já são amplamente relatadas na literatura para síntese de esferas (SHARMA; YNGARD; LIN, 2009), cubos (SHERRY *et al.*, 2006), estrelas (GARCIA-LEIS; GARCIA-RAMOS; SANCHEZ-CORTES, 2013) e prismas (AHERNE *et al.*, 2008; XUE *et al.*, 2008). Aherne *et al*, (2008) propuseram a síntese de nanoprismas através de uma semente estabilizada por polímeros, onde observou-se que a utilização do poli(4-estirenosulfonato) de sódio (PSSS) na produção de pequenas esferas por meio da redução com borohidreto de sódio, que gera defeitos na superfície da partícula e posteriormente, numa segunda redução com ácido ascórbico, os íons Ag^+ ligam-se as faces que não interagem com o polímero, fazendo com que o crescimento seja ordenado e resulte como produto majoritário os nanoprismas de prata.

A Figura 5 mostra o mecanismo de ligação dos íons prata nas sementes esféricas que possuem defeitos, gerando as partículas prismáticas. Por conta da ligação do PSSS nas faces {111} da partícula, a face {100} que está disponível pra a

ligação vai receber as pratas adicionadas, fazendo com que sejam geradas as pontas características dos prismas (AHERNE *et al.*, 2008). Por expressar essas pontas, o efeito de RPS pode ser mais acentuado quando comparado com outras partículas, como as esféricas, e o efeito pode ser mais eficaz (MILLSTONE *et al.*, 2009).

Figura 5 - Mecanismo de ligação dos íons Ag^+ na superfície das partículas esféricas com defeito (seeds), indicando o local onde ocorre essa ligação para a formação das pontas (setas pretas).

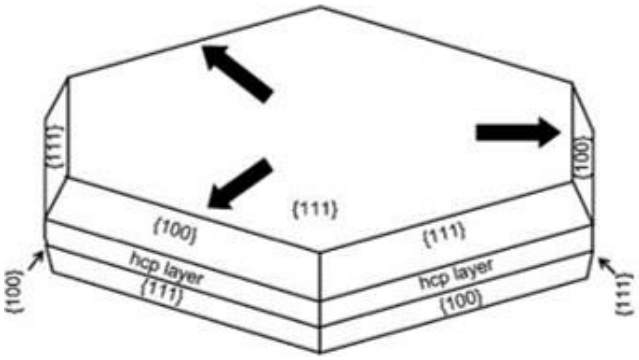

Fonte: Adaptado de Aherne et al, (2008).

3.3.1 Propriedades das nanopartículas de prata

Na interação de um feixe de luz e uma partícula metálica, o campo eletromagnético proveniente induz a oscilação coletiva dos elétrons que estão presentes na superfície das NPs, fenômeno chamado de ressonância localizada de plásmons de superfície (RPS). Basicamente, em intervalos de tempo, ocorre a acumulação de elétrons em uma partícula na direção contrária ao campo gerado, como esquematizado na Figura 6 (a) (AMIRJANI; FATMEHSARI, 2018).

Figura 6 - Esquema do efeito de ressonância de plásmons de superfície de AgNPs (a) e correlaçãotamanho/banda espectral observado para nanoprismas de prata crescidas a partir de esferas (b).

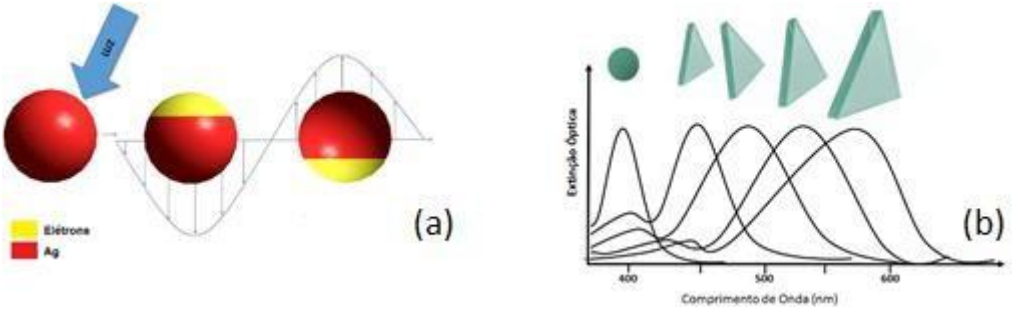

Fonte: Autor (2021).

Esse fenômeno interfere diretamente na posição e intensidade da banda de plásmons da partícula no processo de extinção da luz, e está relacionado com o tamanho e forma obtidas em síntese (LI; CUSHING; WU, 2015). Na Figura 7, é possível observar a correlação entre as diferentes morfologias apresentadas para partículas de prata e o intervalo espectral variável de acordo com o tamanho que elas apresentam. Considerando uma morfologia específica, a banda de extinção desloca-se para regiões maiores de comprimento de onda conforme observamos o aumento do tamanho da partícula. Assim, considerando o máximo de absorção do FS desejado para aplicação, metodologias específicas podem ser empregadas para visando uma sobreposição espectral (JOSHI *et al.*, 2017).

Figura 7 - Relação entre as morfologias de nanopartículas de prata e seus intervalos de extinção na região do visível, compreendendo bandas que podem ser de 300 a 900 nm.

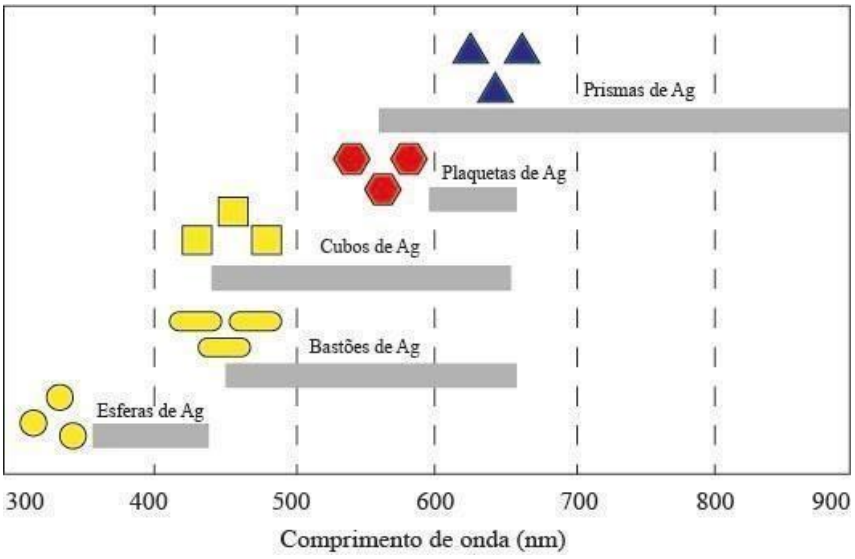

Fonte: Adaptado de Melo (2013).

As bandas de extinção de nanopartículas podem ser classificadas em dois grupos: isotrópicas e anisotrópicas. Na primeira, temos apenas uma banda de extinção e, consequentemente apenas uma banda de plásmon, como é observado para a morfologia esférica. Na anisotropia, é característico a presença de mais de uma banda, tendo então mais de uma ressonância de plásmon, comumente classificados em eixos curto e longo, correspondendo bandas transversais e longitudinais, respectivamente (CAO; SUN; GRATTAN, 2014). Outra propriedade altamente relatada na literatura é a atividade antibacteriana das nanopartículas de prata. Diferentes mecanismos são propostos para esta atividade, como a dissolução

oxidativa, que promove a entrada de íons Ag^+ na célula (LIAO *et al.*, 2019). Entretanto, seu uso na TFD está diretamente relacionado com a RPS e a transferência de energia que decorre do processo.

3.3.2 Mecanismos de amplificação plasmônica

A amplificação plasmônica foi primeiramente relatada em 1991, por meio do primeiro sensor que intensificador de fluorescência, que tornou ponto de partida para o desenvolvimento de novos sistemas, com diferentes condições e composições (LI; CUSHING; WU, 2015). Dois processos podem exemplificar o efeito de amplificação plasmônica, esquematizados na Figura 5.

Após a irradiação de uma partícula por um campo eletromagnético, como a luz, a energia decorrente dos plásmons em movimento na sua superfície é reservada num campo local intenso. Quando temos partículas metálicas pequenas e espalhamento elétrico, essa energia é convertida em calor e é absorvida. Quando temos redução radiativa, ocorre diminuição da banda de plásmon e a energia é re-irradiada a um campo próximo. Então, se essa última hipótese ocorre próximo a um fluoróforo, esta radiação pode ser utilizada para a intensificar sua fluorescência.

O estado excitado do fluoróforo pode ser descrito por um dipolo radiativo, que sofre os fenômenos conhecidos de excitação, relaxação e emissão quando interage com a luz (LI; CUSHING; WU, 2015). A transferência de energia entre a banda de plásmon e a espécie fluorescente também ocorre por interações dipolo-dipolo, e seu mecanismo depende fortemente da distância entre os centros plasmônicos e fluorescentes.

Isto porque enquanto a relaxação radiativa do fluoróforo pode levar um tempo considerável (ns), a relaxação plasmônica é muito mais rápida, e a seção de choque dos elétrons a serem excitados durante o efeito plasmônico é muito baixa também. Desta forma, teoricamente o metal e o centro fluorescente devem ficar numa distância entre 1 a 10 nm um do outro, para que possa haver o efeito de intensificação da fluorescência. Esta situação foi descrita como a transferência de energia de Förster (FRET, Figura 8a) (MERTENS, 2007).

Outro fenômeno também pode ser modelado para este processo: o fenômeno de Purcell (Figura 8b), o qual ocorre preferencialmente para uma distância pouco maior que 10 nm. A superposição espectral entre a banda de plásmon e o fluoróforo determina se o efeito FRET ou Purcell estarão presentes e qual destes mecanismos

levarão ao aumento ou à supressão da fluorescência da espécie. Se a banda de plásmon se superpõe a da absorção do fluoróforo a taxa de excitação do fluoróforo será aumentada. Para nanopartículas que têm um diâmetro menor que 15 nm, o fluoróforo será excitado através de processo FRET pelo intenso campo local plasmônico. Para nanopartículas metálicas maiores que 15 nm o fenômeno FRET prevalece somente a distancias menores que 10 nm, e o efeito Purcell a distancias maiores (10 – 50 nm) (LI; CUSHING; WU, 2015).

Figura 8 - Mecanismos de amplificação da fluorescência via plasmônica que podem ser observadas. O fenômeno FRET (a) - geralmente predominante - e o efeito Purcell (b).

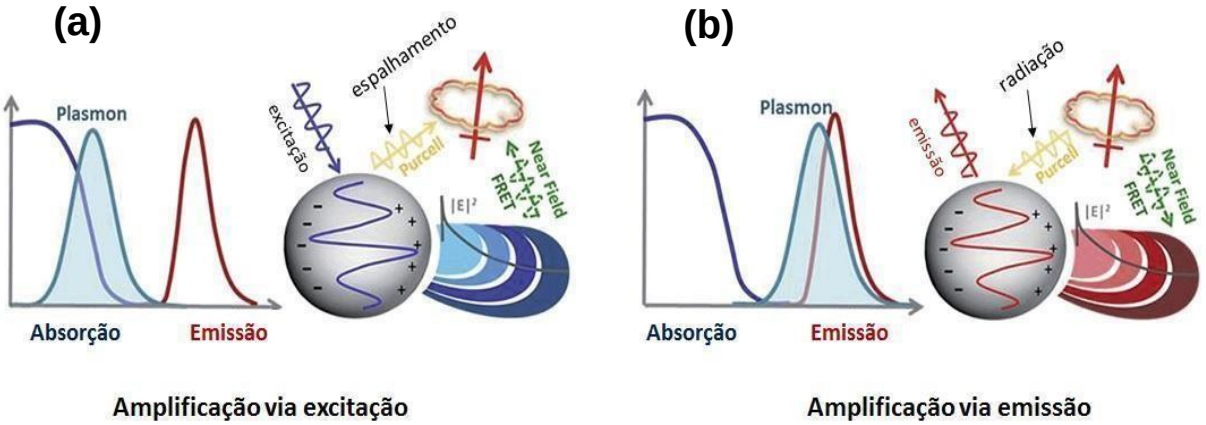

Fonte: Adaptado de Li et al (2015).

4 RESULTADOS E DISCUSSÃO

Os resultados e discussão dos achados dessa pesquisa serão apresentados em formato de artigo, divididos em duas sessões:

Apêndice A – Silver nanoprisms as plasmonic enhancers applied in the photodynamic inactivation of Staphylococcus aureus isolated from bubaline mastitis, publicado em 2021 na **Photodiagnosis and Photodynamic Therapy**, e que descreve os resultados do uso de conjugados de nanoprismas de prata com azul de metileno (na concentração de 45 µmol.L-1) para a inativação da cepa multirresistente isolada da mastite bubalina. Disponível em: https://doi.org/10.1016/j.pdpdt.2021.102315

Apêndice B - Silver nanoprisms@methylene blue conjugates as a strategy against Candida albicans isolated from balanitis in vitro using photodynamic inactivation, a ser submetido ao **Photodiagnosis and Photodynamic Therapy**, e que mostra o potencial dos conjugados (em diferentes concentrações) obtidos frente ao isolado, diminuindo o tempo de inativação necessário quando comparado com o azul de metileno em solução.

5 CONCLUSÃO

Nanoprismas de prata foram obtidos por meio da metodologia já descrita de crescimento por semente, tendo pico máximo de banda de plásmon em 664 nm, para conjugação com o azul de metileno. As análises de MET mostraram um tamanho médio de d = 37 ± 8 nm, e ausência de toxicidade frente a linhagem de macrófagos sadios. Por meio de cálculos teóricos, foi possível observar correlação com a banda de extinção obtida e também visualizar o aumento do campo elétrico para o prisma.

Diferentes conjugados foram preparados: o primeiro com uma [AM] = 45 $\mu mol.L^{-1}$ para a inativação da cepa de *S. aureus* e o segundo com diferentes concentrações (25, 50 e 100 $\mu mol.L^{-1}$) para estudos com a *C. albicans*. Mudanças nos potenciais zetas de superfície indicam que houve mudança na superfície dos prismas por meio da adição do azul de metileno, de carga positiva. Os conjugados obtidos foram altamente estáveis e resistentes a fotodegradação, com perfis de absorção e de emissão dependentes da dose do azul de metileno utilizada. Todos os conjugados tiveram mudanças no perfil de fluorescência comparados com o AM em solução. Aumento de *ca de* 35% foi observado para a [AM] 100 $\mu mol.L^{-1}$ após sua associação aos nanoprismas e acredita-se que esta associação favorece processos de intensificação plasmônica, bem como reduz a auto-supressão da flurescência, bem como fenômeno de dimerização do azul de metileno.

Na inativação, foi observado que a solução de azul de metileno sozinha (25 a 100 $\mu mol.L^{-1}$ não foi capaz de inativar os isolados estudados. Possivelmente, empregando altas doses de luz (prolongando o tempo de irradiação), o efeito seria alcançado. Com os conjugados obtidos e caracterizados no estudo, foi possível observar a inativação em tempos relativamente baixos. Para *S. aureus*, o tempo de inativação utilizando o conjugado foi de 6 minutos, onde apenas o AM só promoveu uma redução da viabilidade no tempo de 9 minutos.

Com a *C. albicans*, a inativação durante todos os tempos testados apenas com o AM não foi satisfatória, também com a redução de 1 log fúngico no tempo de 240s. Para os conjugados, exceto aquele de menor dose do AM, onde não foi observado efeito, foi possível ver um perfil de inativação que diminuía em função do tempo quando se aumentava a concentração do FS. Com a [AM] = 100 $\mu mol.L^{-1}$, foi possível verificar que t = 120s foi suficiente para a morte total da levedura. Com esses dados,

mostramos que os conjugados são excelentes candidatos a fotossensibilizadores para estudos posteriores, ainda *in vitro* e também *in vivo*.

6 PESPECTIVAS

- Determinar a concentração de íons Ag^+ e número de partículas de Ag efetivas presentes nos conjugados;
- Uma vez sabendo essa concentração, realizar estudo com a variação desta e observar sua influência no efeito;
- Estudar o efeito de outras bandas de plásmon que estão após ou antes o máximo de absorção do AM, e verificar a contribuição destas para ou efeito;
- Inativar outras leveduras do gênero *Candida*, como as espécies *Candida tropicalis* e *Candida glabrata*;
- Verificar a eficácia dos conjugados frente a biofilmes, tanto de *C. albicans*, como aqueles mistos com bactérias patogênicas.

REFERÊNCIAS

AHERNE, D. *et al.* Optical Properties and Growth Aspects of Silver Nanoprisms Produced by a Highly Reproducible and Rapid Synthesis at Room Temperature. **Advanced Functional Materials**, 23 jul. 2008. v. 18, n. 14, p. 2005–2016. Disponível em: <https://doi.org/10.1002/adfm.200800233>.

ALBERDI, E.; GÓMEZ, C. Successful treatment of Pityriasis Versicolor by photodynamic therapy mediated by methylene blue. **Photodermatology, Photoimmunology & Photomedicine**, 19 mar. 2020. v. n/a, n. n/a. Disponível em: <https://doi.org/10.1111/phpp.12555>.

ALVARENGA, Letícia Heineck *et al.* Aggregatibacter actinomycetemcomitans biofilm can be inactivated by methylene blue-mediated photodynamic therapy. **Photodiagnosis and Photodynamic Therapy**, 1 mar. 2015. v. 12, n. 1, p. 131–135.

AMIRJANI, A.; FATMEHSARI, D. H. Colorimetric detection of ammonia using smartphones based on localized surface plasmon resonance of silver nanoparticles. **Talanta**, 2018. v. 176, p. 242–246. Disponível em: <http://www.sciencedirect.com/science/article/pii/S0039914017308421>.

BAPTISTA, A. *et al.* **Antimicrobial Photodynamic Therapy as a Strategy to Arrest Enamel Demineralization: A Short-Term Study on Incipient Caries in a Rat Model**. [S.l.]: [s.n.], 2011. V. 88.

BARBER, D.; FREESTONE, I. **An investigation of the origin of the colour of the Lycurgus Cup by analytical TEM**. [S.l.]: [s.n.], 2007. V. 32.

BEN-AMI, R. **Treatment of Invasive Candidiasis: A Narrative Review**. **Journal of Fungi** .

BERTOLINI, M. *et al.* Candida albicans induces mucosal bacterial dysbiosis that promotes invasive infection. **PLOS Pathogens**, 22 abr. 2019. v. 15, n. 4, p. e1007717. Disponível em: <https://doi.org/10.1371/journal.ppat.1007717>.

BUSH, K. *et al.* Tackling antibiotic resistance. **Nature Reviews Microbiology**, 2011. v. 9, n. 12, p. 894–896. Disponível em: <https://doi.org/10.1038/nrmicro2693>.

CABRAL, F. V *et al.* Preclinical Investigation of Methylene Blue-mediated Antimicrobial Photodynamic Therapy on Leishmania Parasites Using Real-Time Bioluminescence. **Photochemistry and Photobiology**, 1 maio. 2020. v. 96, n. 3, p. 604–610. Disponível em: <https://doi.org/10.1111/php.13188>.

CAO, J.; SUN, T.; GRATTAN, K. T. V. Gold nanorod-based localized surface plasmon

resonance biosensors: A review. **Sensors and Actuators B: Chemical**, 1 maio. 2014. v. 195, p. 332–351. Disponível em: <https://www.sciencedirect.com/science/article/pii/S0925400514000732>. Acesso em: 19 maio 2019.

CIEPLIK, F. *et al.* Antimicrobial photodynamic therapy – what we know and what we don't. **Critical Reviews in Microbiology**, 3 set. 2018. v. 44, n. 5, p. 571–589. Disponível em: <https://doi.org/10.1080/1040841X.2018.1467876>.

CLEARY, I. A. *et al.* Examination of the pathogenic potential of Candida albicans filamentous cells in an animal model of haematogenously disseminated candidiasis. **FEMS Yeast Research**, 1 mar. 2016. v. 16, n. 2, p. fow011. Disponível em: <https://doi.org/10.1093/femsyr/fow011>.

CORREIA, J. H. *et al.* **Photodynamic Therapy Review: Principles, Photosensitizers, Applications, and Future Directions**. **Pharmaceutics** .

COSTA, L. D. Da S. **Síntese e Caracterização de Porfirinas como Potenciais Agentes Fotossensibilizadores em Terapia Fotodinâmica**.

DADAR, M. *et al.* Candida albicans - Biology, molecular characterization, pathogenicity, and advances in diagnosis and control – An update. **Microbial Pathogenesis**, 2018. v. 117, p. 128–138. Disponível em: <https://www.sciencedirect.com/science/article/pii/S0882401017317175>.

DJORDJEVIC, Z. M. *et al.* Health care–acquired infections in neonatal intensive care units: Risk factors and etiology. **American Journal of Infection Control**, 2015. v. 43, n. 1, p. 86–88. Disponível em: <https://www.sciencedirect.com/science/article/pii/S0196655314012140>.

DODDS, D. R. Antibiotic resistance: A current epilogue. **Biochemical Pharmacology**, 2017. v. 134, p. 139–146. Disponível em: <https://www.sciencedirect.com/science/article/pii/S0006295216304671>.

FRANCI, G. *et al.* **Silver Nanoparticles as Potential Antibacterial Agents**. **Molecules** .

GAJDÁCS, M. *et al.* Epidemiology of candiduria and Candida urinary tract infections in inpatients and outpatients: results from a 10-year retrospective survey. **Central European journal of urology**, 2019. v. 72, n. 2, p. 209–214. Disponível em: <https://pubmed.ncbi.nlm.nih.gov/31482032>.

GARCIA-DIAZ, M.; HUANG, Y.-Y.; HAMBLIN, M. R. Use of fluorescent probes for ROS to tease apart Type I and Type II photochemical pathways in photodynamic therapy.

Methods (San Diego, Calif.), 15 out. 2016. v. 109, p. 158–166. Disponível em: <https://pubmed.ncbi.nlm.nih.gov/27374076>.

GARCIA-LEIS, A.; GARCIA-RAMOS, J. V.; SANCHEZ-CORTES, S. Silver Nanostars with High SERS Performance. **The Journal of Physical Chemistry C**, 18 abr. 2013. v. 117, n. 15, p. 7791–7795. Disponível em: <https://doi.org/10.1021/jp401737y>.

GOMES, F.; HENRIQUES, M. Control of Bovine Mastitis: Old and Recent Therapeutic Approaches. **Current Microbiology**, 2016. v. 72, n. 4, p. 377–382. Disponível em: <https://doi.org/10.1007/s00284-015-0958-8>.

GONZÁLEZ-DELGADO, J. A. *et al.* Use of Photosensitizers in Semisolid Formulations for Microbial Photodynamic Inactivation. **Journal of Medicinal Chemistry**, 26 maio. 2016. v. 59, n. 10, p. 4428–4442. Disponível em: <https://doi.org/10.1021/acs.jmedchem.5b01129>.

HABIBIAN DEHKORDI, S.; HOSSEINPOUR, F.; KAHRIZANGI, A. An in vitro evaluation of antibacterial effect of silver nanoparticles on Staphylococcus aureus isolated from bovine subclinical mastitis. **African Journal of Biotechnology**, 12 set. 2011. v. 10.

HEIKKILÄ, A.-M. *et al.* Pathogen-specific production losses in bovine mastitis. **Journal of Dairy Science**, 1 out. 2018. v. 101, n. 10, p. 9493–9504. Disponível em: <https://doi.org/10.3168/jds.2018-14824>.

HOEKSTRA, J. *et al.* Differences between Staphylococcus aureus lineages isolated from ovine and caprine mastitis but not between isolates from clinical or subclinical mastitis. **Journal of Dairy Science**, 1 jun. 2019. v. 102, n. 6, p. 5430–5437. Disponível em: <https://www.sciencedirect.com/science/article/pii/S0022030219303509>. Acesso em: 19 maio 2019.

HU, Yongxuan *et al.* A Case Report of Penile Infection Caused by Fluconazole- and Terbinafine-Resistant Candida albicans. Netherlands: **Mycopathologia**, abr. 2017. v. 182, n. 3–4, p. 397–402.

ITRI, R.; UCHOA, A. F.; BAPTISTA, M. Da S. Princípios da terapia fotodinâmica. **PDT - Terapia fotodinâmica antimicrobiana na odontologia PP - Rio de Janeiro**. [S.l.]: Elsevier, 2013.

JEGADISH, N. *et al.* A descriptive study of the clinical and etiological profile of balanoposthitis. **Journal of Family Medicine and Primary Care**, 2021. v. 10, n. 6. Disponível em: <https://journals.lww.com/jfmpc/Fulltext/2021/10060/A_descriptive_study_of_the_clini

cal_and.24.aspx>.

JESUS, V. P. S. *et al.* Nanoparticles of methylene blue enhance photodynamic therapy. **Photodiagnosis and Photodynamic Therapy**, 2018. v. 23, p. 212–217. Disponível em: <http://www.sciencedirect.com/science/article/pii/S1572100018300449>.

JOSHI, D. N. *et al.* Efficient light harvesting in dye sensitized solar cells using broadband surface plasmon resonance of silver nanoparticles with varied shapes and sizes. **Materials Letters**, 2017. v. 193, p. 288–291. Disponível em: <http://www.sciencedirect.com/science/article/pii/S0167577X17301921>.

KAUFFMAN, C. A. Fungal Infections BT - Infectious Disease in the Aging: A Clinical Handbook. *In*: NORMAN, D.; YOSHIKAWA, T. (Org.). Totowa, NJ: Humana Press, 2009, p. 347–366.

LEAL, C. R. L. *et al.* Antimicrobial photodynamic therapy on Streptococcus mutans is altered by glucose in the presence of methylene blue and red LED. **Photodiagnosis and Photodynamic Therapy**, 2017. v. 19, p. 1–4. Disponível em: <http://www.sciencedirect.com/science/article/pii/S1572100016302733>.

LEE, Y. *et al.* Antifungal Drug Resistance: Molecular Mechanisms in Candida albicans and Beyond. **Chemical Reviews**, 24 mar. 2021. v. 121, n. 6, p. 3390–3411. Disponível em: <https://doi.org/10.1021/acs.chemrev.0c00199>.

LI, M.; CUSHING, S. K.; WU, N. Plasmon-enhanced optical sensors: a review. **Analyst**, 2015. v. 140, n. 2, p. 386–406. Disponível em: <http://dx.doi.org/10.1039/C4AN01079E>.

LIAO, S. *et al.* Antibacterial activity and mechanism of silver nanoparticles against multidrug-resistant Pseudomonas aeruginosa. **International journal of nanomedicine**, 25 fev. 2019. v. 14, p. 1469–1487. Disponível em: <https://pubmed.ncbi.nlm.nih.gov/30880959>.

LISBOA, C. *et al.* Candida balanitis: risk factors. **Journal of the European Academy of Dermatology and Venereology**, 1 jul. 2010. v. 24, n. 7, p. 820–826. Disponível em: <https://doi.org/10.1111/j.1468-3083.2009.03533.x>.

LOHSE, M. B. *et al.* Development and regulation of single- and multi-species Candida albicans biofilms. **Nature Reviews Microbiology**, 2018. v. 16, n. 1, p. 19–31. Disponível em: <https://doi.org/10.1038/nrmicro.2017.107>.

MEDEIROS, E. S. *et al.* Bubaline mastitis etiology in Northeast of Brazil. **Arquivo Brasileiro de Medicina VeterinÃ!`ria e Zootecnia**, 2013. v. 65, p. 1891–1894.

Disponível em: <http://www.scielo.br/scielo.php?script=sci_arttext&pid=S0102-09352013000600043&nrm=iso>.

MELO, L. S. A. DE *et al.* Singlet Oxygen Generation Enhanced by Silver-Pectin Nanoparticles. **Journal of Fluorescence**, 2012. v. 22, n. 6, p. 1633–1638. Disponível em: <https://doi.org/10.1007/s10895-012-1107-4>.

MERTENS, H. **Plasmon-enhanced luminescence near noble-metal nanospheres: Comparison of exact theory and an improved Gersten and Nitzan model**. [S.l.]: [s.n.], 2007. V. 76.

MILLSTONE, J. E. *et al.* Colloidal Gold and Silver Triangular Nanoprisms. **Small**, 20 mar. 2009. v. 5, n. 6, p. 646–664. Disponível em: <https://doi.org/10.1002/smll.200801480>.

MOREIRA, L. H. *et al.* Use of photodynamic therapy in the treatment of bovine subclinical mastitis. **Photodiagnosis and Photodynamic Therapy**, 1 mar. 2018. v. 21, p. 246–251. Disponível em: <https://www.sciencedirect.com/science/article/abs/pii/S1572100017304726>. Acesso em: 19 maio 2019.

NEMEZIO, M. A. *et al.* Effect of methylene blue-induced photodynamic therapy on a Streptococcus mutans biofilm model. **Photodiagnosis and Photodynamic Therapy**, 2017. v. 20, p. 234–237. Disponível em: <http://www.sciencedirect.com/science/article/pii/S1572100017302910>.

PAOLI, J. *et al.* Penile intraepithelial neoplasia: results of photodynamic therapy. Sweden: **Acta dermato-venereologica**, 2006. v. 86, n. 5, p. 418–421.

PARASURAMAN, P. *et al.* **Biogenic Silver Nanoparticles Decorated with Methylene Blue Potentiated the Photodynamic Inactivation of Pseudomonas aeruginosa and Staphylococcus aureus**. **Pharmaceutics** .

PHAM, T. C. *et al.* Recent Strategies to Develop Innovative Photosensitizers for Enhanced Photodynamic Therapy. **Chemical Reviews**, 10 nov. 2021. v. 121, n. 21, p. 13454–13619. Disponível em: <https://doi.org/10.1021/acs.chemrev.1c00381>.

PINHATI, H. M. S. Surto de candidemia por Candida parapsilosis resistente ao fluconazol, em um hospital em Brasília: Caracterização clínica, molecular e avaliação dos fatores associados. 2015. p. 107.

PINTO, J. G. *et al.* Evaluation of methylene blue as photosensitizer in promastigotes of Leishmania major and Leishmania braziliensis. **Photodiagnosis and Photodynamic Therapy**, 2017. v. 18, p. 325–330. Disponível em:

<http://www.sciencedirect.com/science/article/pii/S1572100016302587>.

PRASAD, R.; NAIR, R.; BANERJEE, A. Emerging Mechanisms of Drug Resistance in Candida albicans BT - Yeasts in Biotechnology and Human Health: Physiological Genomic Approaches. *In*: SÁ-CORREIA, I. (Org.). Cham: Springer International Publishing, 2019, p. 135–153.

QAZI, U.; JAVAID, R. **A Review on Metal Nanostructures: Preparation Methods and Their Potential Applications**. [S.l.]: [s.n.], 2016. V. 05.

RIBEIRO, Martha S *et al.* Photodynamic inactivation assisted by localized surface plasmon resonance of silver nanoparticles: In vitro evaluation on Escherichia coli and Streptococcus mutans. **Photodiagnosis and Photodynamic Therapy**, 2018. v. 22, p. 191–196. Disponível em: <http://www.sciencedirect.com/science/article/pii/S1572100017304118>.

RUEGG, P. L. A 100-Year Review: Mastitis detection, management, and prevention. **Journal of Dairy Science**, 2017. v. 100, n. 12, p. 10381–10397. Disponível em: <http://www.sciencedirect.com/science/article/pii/S0022030217310329>.

SEBRÃO, C. C. N. *et al.* Comparison of the Efficiency of Rose Bengal and Methylene Blue as Photosensitizers in Photodynamic Therapy Techniques for Enterococcus faecalis Inactivation. **Photomedicine and Laser Surgery**, 9 set. 2016. v. 35, n. 1, p. 18–23. Disponível em: <https://doi.org/10.1089/pho.2015.3995>.

SHARMA, V. K.; YNGARD, R. A.; LIN, Y. Silver nanoparticles: Green synthesis and their antimicrobial activities. **Advances in Colloid and Interface Science**, 30 jan. 2009. v. 145, n. 1–2, p. 83–96. Disponível em: <https://www.sciencedirect.com/science/article/pii/S0001868608001449>. Acesso em: 19 maio 2019.

SHERRY, L. J. *et al.* Localized Surface Plasmon Resonance Spectroscopy of Single Silver Triangular Nanoprisms. **Nano Letters**, 1 set. 2006. v. 6, n. 9, p. 2060–2065. Disponível em: <https://doi.org/10.1021/nl061286u>.

SILVA, J. M. *et al.* Atividade antimicrobiana de moléculas bioativas produzidas por Streptomyces parvulus DPUA 1573 frente a Staphylococcus spp. multirresistentes de mastite bubalina. **Pesquisa Veterinária Brasileira**, set. 2016. v. 36, n. 9, p. 805–810. Disponível em: <http://www.scielo.br/scielo.php?script=sci_arttext&pid=S0100-736X2016000900805&lng=pt&tlng=pt>. Acesso em: 20 maio 2019.

SILVA, M. O. DA; AQUINO, S. Resistência aos antimicrobianos: uma revisão dos desafios na busca por novas alternativas de tratamento. **Revista de Epidemiologia e**

Controle de Infecção, 8 out. 2018. v. 8, n. 4 SE-, p. 472–482. Disponível em: <https://online.unisc.br/seer/index.php/epidemiologia/article/view/11580>.

SILVESTRE, A. L. P. *et al.* Current applications of drug delivery nanosystems associated with antimicrobial photodynamic therapy for oral infections. **International Journal of Pharmaceutics**, 2021. v. 592, p. 120078. Disponível em: <https://www.sciencedirect.com/science/article/pii/S0378517320310632>.

SPEZZIA-MAZZOCCO, T. *et al.* In-vitro effect of antimicrobial photodynamic therapy with methylene blue in two different genera of dermatophyte fungi. Berlin, Boston: **Photonics & Lasers in Medicine**, 2016. v. 5, n. 3, p. 203–210. Disponível em: <https://www.degruyter.com/view/journals/plm/5/3/article-p203.xml>.

SREDNIK, M. E. *et al.* Characterisation of *Staphylococcus aureus* strains isolated from mastitis bovine milk in Argentina. **Journal of Dairy Research**, 22 fev. 2018. v. 85, n. 1, p. 57–63. Disponível em: <https://www.cambridge.org/core/product/identifier/S0022029917000851/type/journal_article>. Acesso em: 19 maio 2019.

TOKUBO, L. M. *et al.* Antimicrobial effect of photodynamic therapy using erythrosine/methylene blue combination on Streptococcus mutans biofilm. **Photodiagnosis and Photodynamic Therapy**, 2018. v. 23, p. 94–98. Disponível em: <http://www.sciencedirect.com/science/article/pii/S1572100017303290>.

VIANA, O. De S. Desenvolvimento de sistemas nanoestruturados à base de quantum dots livres e associados a porfirinas para aplicação em terapia fotodinâmica. 2015.

VIDHU, V. K.; PHILIP, D. Catalytic degradation of organic dyes using biosynthesized silver nanoparticles. **Micron**, 1 jan. 2014. v. 56, p. 54–62. Disponível em: <https://www.sciencedirect.com/science/article/pii/S0968432813001704>. Acesso em: 19 maio 2019.

WALL, G. *et al.* Candida albicans biofilm growth and dispersal: contributions to pathogenesis. **Current Opinion in Microbiology**, 2019. v. 52, p. 1–6. Disponível em: <https://www.sciencedirect.com/science/article/pii/S1369527418300973>.

XUE, C. *et al.* Mechanistic Study of Photomediated Triangular Silver Nanoprism Growth. **Journal of the American Chemical Society**, 1 jul. 2008. v. 130, n. 26, p. 8337–8344. Disponível em: <https://doi.org/10.1021/ja8005258>.

YANG, S. M. *et al.* Hydrogen Peroxide Enhances the Antibacterial Effect of Methylene Blue-based Photodynamic Therapy on Biofilm-forming Bacteria. **Photochemistry and Photobiology**, 1 maio. 2019. v. 95, n. 3, p. 833–838. Disponível em:

<https://doi.org/10.1111/php.13056>.

ZHANG, Ying; ERKEY, C. Preparation of supported metallic nanoparticles using supercritical fluids: A review. **The Journal of Supercritical Fluids**, 2006. v. 38, n. 2, p. 252–267. Disponível em: <http://www.sciencedirect.com/science/article/pii/S0896844606001021>.

APÊNDICE A - ARTIGO 1 – SILVER NANOPRISMS AS PLASMONIC ENHANCERS APPLIED IN THE PHOTODYNAMIC INACTIVATION OF STAPHYLOCOCCUS AUREUS ISOLATED FROM BUBALINE MASTITIS

Publicado na Photodiagnosis and Photodynamic Therapy
Fator de impacto: 3.6 (2020) – Qualis de área (Farmácia): A2

Photodiagnosis and Photodynamic Therapy 34 (2021) 102315

Contents lists available at ScienceDirect

Photodiagnosis and Photodynamic Therapy

journal homepage: www.elsevier.com/locate/pdpdt

Silver nanoprisms as plasmonic enhancers applied in the photodynamic inactivation of *Staphylococcus aureus* isolated from bubaline mastitis

Cláudio H. Rodrigues [a], Evanísia A.G. Araújo [a], Rômulo P. Almeida [a], Thiago P. Nascimento [b], Marllyn M. Silva [c], Ghulam Abbas [d], Frederico D. Nunes [e], Emery Lins [f], Mariane C. B. Lira-Nogueira [c], Juliana S.A. Falcão [g], Adriana Fontes [h], Ana L.F. Porto [b], Goreti Pereira [i], Beate S. Santos [a,*]

[a] Pharmaceutical Sciences Department, Federal University of Pernambuco, Recife, PE, Brazil
[b] Morphology and Animal Physiology Department, Federal Rural University of Pernambuco, Recife, PE, Brazil
[c] Academic Center of Vitória, Federal University of Pernambuco, Vitória, PE, Brazil
[d] Department of Physics, Riphah International University Faisalabad Campus, Pakistan
[e] Nuclear Engineering Department, Federal University of Pernambuco, Recife, PE, Brazil
[f] Electronic and Systems Department, Federal University of Pernambuco, Recife, PE, Brazil
[g] Education and Health Center, Federal University of Campina Grande, Cuité, PB, Brazil
[h] Biophysics and Radiobiology Department, Federal University of Pernambuco, Recife, PE, Brazil
[i] Fundamental Chemistry Department, Federal University of Pernambuco, Recife, PE, Brazil

ARTICLE INFO

Keywords:
Methylene blue
Metallic nanoprismatic platelets
Photodynamic therapy
Bacterial infection

ABSTRACT

Mastitis is a bacterial infection that affects all lactating mammals, and in dairy cattle, it leads to a reduction in their milk production and, in worse cases, it may lead to animal death. One viable therapeutic modality for overcoming bacterial resistance can be photodynamic inactivation (PDI), a therapeutic modality for bacterial infection treatment. One of the main factors that can lead to an efficient PDI process is the association of metallic nanoparticles in the close vicinity of photosensitizers, which has shown promising results due to localized surface plasmon resonance phenomena. In this work, methylene blue (MB) molecules were associated with Ag prismatic nanoplatelets (AgNPrs) to use as PDI photosensitizer against *Staphylococcus aureus* isolated from bubaline mastitis. The optical plasmonic activity of AgNPrs was tuned to the MB absorption region (600–700 nm) by inducing their growth into prismatic shapes by a seed-mediated procedure, using poly (sodium 4-styrene sulfonate) as the surfactant. A simulation on the plasmonic properties of the nanoprisms, applying particle size within the dimensions determined by TEM image analysis ($d = 32 \pm 6$ nm), showed a 30 % increase of the incident field on the prismatic tips. Photodynamic results showed that the electrostatic AgNPr-MB conjugates promoted enhancement (*ca.* 15 %) of the reactive oxygen species production. Besides, PDI mediated by AgNPrs–MB led to the complete inactivation of the mastitis *S. aureus* strain after 6 min inactivation, in contrast to PDI mediated by MB, which reduced less than a 0.5 bacterial log. Thus, the results show this plasmonic enhanced photodynamic tool's potential to be applied in the inactivation of multi-resistant bacterial strains.

1. Introduction

Mastitis is an acute inflammation of the mammary glands, which currently affects a wide range of mammals. This pathology can cause the reduction of milk production, also changing its composition and quality [1] and, in worst cases if sepsis occurs, it can be fatal. Thus, it has a strong relationship with the economy since milk is a primary feedstock for foods. Bacterial resistance, which has been increasing in recent years, is a significant concern for the industry, leading to antibiotics ineffectiveness in these cases [2,3]. Besides cattle, the disease can also affect buffaloes and small ruminants, being the clinic treatment dependent on the virulence of the strain and the host responsiveness [4,5].

The main microorganism associated with these infections is *Staphylococcus aureus*. Moreover, other pathogens can be part of the microbiota

* Corresponding athor.
E-mail address: beate.santos@ufpe.br (B.S. Santos).

https://doi.org/10.1016/j.pdpdt.2021.102315
Received 19 January 2021; Received in revised form 4 April 2021; Accepted 23 April 2021
Available online 28 April 2021

and be involved in the disorder, such as *Streptococcus uberis*, *Escherichia coli*, and *Klebsiella* spp. [1]. Among the possible treatments to combat mastitis, the use of antibiotics stands out. However, in the last years, with the emergence of resistant bacteria, alternative and practical techniques that do not cause resistance to microorganisms are being tested. Among these strategies, photodynamic therapy (PDT), a technology that combines a light-sensitive substance (photosensitizer - PS) and a light source, is very well known to effectively inactivate pathogens [6–8]. The cell death is due to the light activation of PS molecules, which promotes the formation of reactive oxygen species (ROS) in the presence of molecular oxygen [9]. PDT has emerged as a potential treatment for pathogens in a modality called photodynamic inactivation (PDI) [10, 11]. This technique has shown inactivation effectiveness for a diverse range of microorganisms, such as bacteria [12,13], fungi [14,15], and parasites [16,17].

Furthermore, a significant number of metallic nanoparticles (NPs) such as silver (Ag), gold (Au), and copper (Cu), and their binary and ternary compositions, have localized surface plasmon resonance (LSPR) bands as a unique optical property [18]. This LSPR effect results from electrons' collective oscillation present at the metallic interfaces, upon interacting with electromagnetic radiation, for example, in the visible spectrum range [19,20]. This property is highly dependent on the size and shape of the NPs, leading to an enhancement on the electric field intensity near the NP surface, influencing any molecule or particle nearby. This electric field enhancement has been shown to improve various species' optical properties, such as luminescence of carboxyl-coated CdTe quantum dots [21]. This phenomenon is mediated by dipole-dipole interactions and occurs through different mechanisms [22].

The use of metallic NPs for PDT has already been previously explored to induce the enhancement of ROS generation by different processes. Ag and Au nanostructures are continuously being tested for that purpose in PDT for cancer cells/tissues and PDI of pathologic bacterial strains. For example, Ag nanoclusters were used to enhance singlet oxygen generation in the presence of the Rose Bengal dye and promoted full *in vitro* eradication of oral bacterial cells [23]. Ag nanospheres were combined with Riboflavin to study their enhanced capacity for bacterial inactivation [24,25]. Ag NPs were also used to functionalize porphyrins and increased their photodynamic potential for the inactivation of *S. aureus* strains [26] and treating the melanoma cancer cell line [27]. More recently, Jesus and coll. (2018) [28] showed that they were able to increase carcinoma cell death by applying methylene blue (MB) molecules in the presence of either Au or Ag nanospheres. These authors stated that the cytotoxicity effect of MB associated with AgNPs on the MDA-MB-468 cell line could be related to increased ROS production. Khoza et al. (2020) [29] applied a novel metal-free phthalocyanine with spheric AgNPs and observed an increase of photodynamic action in cell melanoma cancer cell line. In all of these studies, spherical Ag NPs were applied to associate with PS. Indeed, Ag NPs and their composites, show very interesting surface mediated light interaction processes enabling applications associated to energy transfer processes and as active components for heterogeneous catalysis [30–32]. One of the mechanisms that induce plasmonic enhancement of optical features, such as fluorescence, is the known Forster energy transfer (FRET) process. To guarantee the FRET mechanism, two main conditions must be taken into account: (i) molecule-NP distance must be lower than 10 nm, and (ii) the maximum electronic absorption band of the acceptor and the maximum of the plasmonic band (donor) must show a good spectral overlap [33].

Thus, in this context, this work aims to show that, by optically coupling Ag nanoprisms (AgNPr) to MB, a very known and safe PS under dark condition [34], we may enhance the photoinactivation of a multi-resistant strain of *S. aureus* isolated from bubaline mastitis by inducing the plasmonic field enhancement due to Forster mechanism. The *S. aureus* strain applied here tested positive for beta-lactamase, as well as negative for coagulase and, moreover, showed high resistance to different antibiotics has been reported, such as ampicillin (85 %), penicillin (93 %), sulfonamides (89 %), novobiocin (89 %), lincomycin (76 %), kanamycin (79 %), streptomycin (63 %), erythromycin (61 %), and oxacillin (81 %) [35]. So, aiming at FRET-induced fluorescence enhancement for PDI applications, in the present study, we tuned the spectral profile of Ag NPs to overlap the absorption spectrum of MB by inducing their non-isotropic growth into prismatic nanoplatelets. Applying polystyrene poly(sodium 4-styrene sulfonate) (PSSS) polymer as seed surfactant we, not only induced the Ag spherical seeds to grow into Ag prismatic nanoplatelets (AgNPr) but, we also promoted electrostatic interactions of the negative AgNPr to the positive MB molecules, guaranteeing their proximity (as schematized in Fig. 1). From our knowledge, this is the first report on applying prismatic Ag NPs for this purpose.

2. Materials and methods

2.1. Materials

All chemicals were used as received without further purification. Trisodium citrate (TSC, 98 % purity), poly (sodium 4-styrene sulfonate) (PSSS, 70 kDa), sodium borohydride ($NaBH_4$, 98 % purity), silver nitrate ($AgNO_3$, 98 % purity), *N,N*-dimethyl-4-nitrosoaniline (RNO, 97 %), L-Histidine (L-His, 99 %), polyvinyl alcohol (PVA, 89−90 kDa) were purchased from Sigma-Aldrich (St. Louis, MO, USA). Methylene blue (99 %) was purchased from Merck. Ascorbic acid was purchased from Neon Comercial (Suzano, São Paulo, Brazil). Nutrient broth and Mueller-Hinton agar were purchased from Himedia (Kennett Square, Pennsylvania, USA).

2.2. Synthesis of seed-mediated Ag nanoprisms

Ag NPs were prepared following the methodology described by Aherne et al. [36] with minor adaptations. In a typical experiment, Ag seeds were produced in an aqueous medium, at room temperature (RT −25 °C), mixing under vigorous stirring a solution of TSC (5.0 mL, 2.5 $mmol \cdot L^{-1}$, PSSS 0.25 mL, 500 mg L^{-1}), and $NaBH_4$ (0.3 mL, 10 $mmol \cdot L^{-1}$, freshly prepared), followed by dropwise addition of $AgNO_3$ (5.0 mL, 0.5 $mmol \cdot L^{-1}$). The system was kept under stirring for 3 min.

Silver prismatic nanoplatelets were obtained by adding deionized water (5.0 mL) and ascorbic acid (75 μL, 10 $mmol \cdot L^{-1}$) to three different volumes of the Ag seed suspension (650, 400, and 200 μL), followed by addition of $AgNO_3$ (3.0 mL, 0.5 $mmol \cdot L^{-1}$), under vigorous stirring, at RT, for 3 min.

2.3. Physico-chemical characterization of AgNPrs

The Ag nanostructures were characterized by UV–vis spectroscopy (Evolution 600S, Thermo Fisher), in the 350–800 nm region, to monitor the plasmon bands for the seeds and AgNPrs.

Transmission electron microscopy images were acquired in a Spirit Biotwin G2 at 120 kV (FEI Tecnai G^2 Spirit Biotwin), coupled to a CD MegaView Olympus 2 K and Eagle 4 K camera or in a F20 HRTEM at 200 kV (FEI Tecnai G^2 F20 HRTEM). Samples were prepared by dropping *ca.* 10 μL of the concentrated Ag NP suspension on a copper grid and letting it dry before the visualization. Morphological aspects of the images were analyzed using ImageJ software. The particles' size (d) was defined by their longitudinal length (obtained from one tip to the opposite base), and the width was obtained by measuring laterally piled particles.

X-ray Diffraction measurements of AgNPr3 samples were acquired in a XRD-7000 (Shimadzu) equipment, applying CuKα radiation wavelength (1.548 Å) and a voltage of 40 kV. For this, concentrated AgNPr3 samples were dispersed in a 1% polyvinyl alcohol (PVA) solution and dried into a film under vacuum [36,37]. PVA sample was also measured. FT-IR spectra of the AgNPr3 sample embedded in PVA film was recorded using an attenuated total reflectance (ATR) technique in a Cary 630 FTIR (Agilent Technologies) Spectrometer. FT-IR spectra of PSSS and PVA

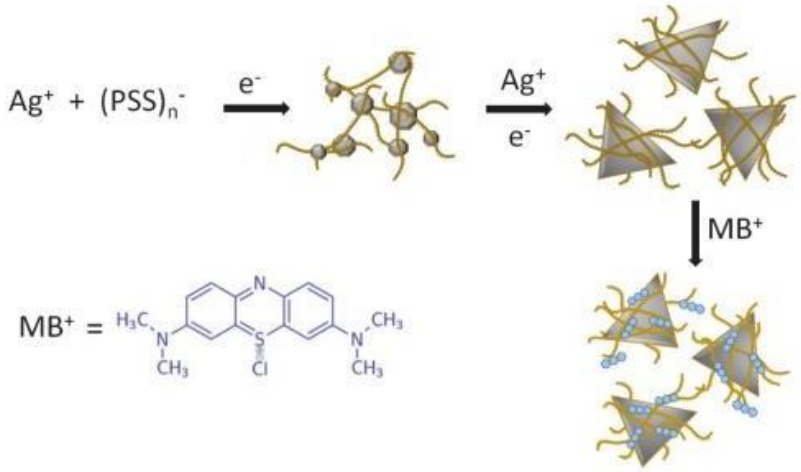

Fig. 1. Short scheme depicting silver nanoprisms stabilized by poly (4-styrene sulfonate) sodium anionic polymers in aqueous medium and their association to positive methylene blue for plasmonic enhanced photodynamic action.

film samples were also acquired.

2.4. Numerical modeling for AgNPrs

The simulation of Ag particles was performed using the finite element method (FEM) with COMSOL Multiphysics. A spherical perfectly-matched-layer 10 times greater than the length (d) of nanoprism was used to enclose the simulation volume. To avoid unnecessary reflections, other proper boundary conditions were applied to study the nature of nanoprism. Optical data from Johnson and Christy [38] were used to model the dielectric functions of AgNPrs. During the simulations, water was considered as a surrounding medium with a refractive index of 1.33. The magnitude of the background electric field was set at 1 V/m for all nanoparticles.

2.5. Association of AgNPrs with methylene blue (AgNPr-MB)

Ag nanoprisms were first centrifuged (1400 ×g at 4 °C) for 15 min, and the pellet was dispersed in deionized water to reduce residual precursor species. An aqueous MB stock solution was prepared using phosphate saline-buffered (PBS, pH 7.2) and filtered using a sterile membrane (0.22 μm). Then, under stirring, MB solution was added to the AgNPr suspension to obtain a final concentration of the photosensitizer of 45 $\mu mol \cdot L^{-1}$. The mixture was left stirring overnight at RT. AgNPr-MB systems were characterized by UV–vis spectroscopy (Evolution 600S, Thermo Fisher) in the spectral region of 350–800 nm. The emission spectra were recorded in a fluorescence spectrometer (PerkinElmer, model LS55). Before characterization, the AgNPr-MB nanosystems were purified by centrifugation (1900 ×g, 15 min) and then redispersed in deionized water. All manipulation regarding MB was performed in the dark.

The Zeta potential (ζ) of AgNPr and AgNPr-MB nanosystems were measured using Zetasizer Nanoseries s90 equipment (Malvern Panalytical) after sample purification using a filter concentrator with a molecular weight cut off of 10 kDa (General Eletrics®). The volume of 5 mL of each system was added to 50 mL of deionized water, and the samples were sonicated for 30 min. An aliquot of 1 mL of each system was used for the analysis. The ζ measurements were performed in triplicate by diluting the samples at the same concentration using deionized water. The same procedure was performed with the Ag nanoprisms.

2.6. In vitro reactive oxygen species (ROS) quantification

The production of ROS was analyzed using the indirect chemical method, utilizing RNO and L-His [39]. For this, 1 mL of MB solution (15 $\mu mol \cdot .L^{-1}$) or the nanosystem suspension was added to a quartz cuvette, containing 1 mL of RNO (39 $\mu mol \cdot L^{-1}$) and 1 mL of L-His (45 $mmol \cdot L^{-1}$). Then, the samples were irradiated up to 300 s either by 20 s or 60 s irradiation periods, using a red LED (Blackbox Smart, coupled with LEDbox λ = 660 nm and Light Chamber, BioLambda®) with an irradiance of 45.8 $mW \cdot cm^{-2}$ (*i.e.*, for 300 s, radiant exposure reached was *ca.* 12 $J \cdot cm^{-2}$). Each sample was analyzed by UV–vis spectroscopy, observing the band at λ = 440 nm, which corresponds to the RNO maximum absorption. Measurements without AgNPrs were realized as a control, and the ROS percentage was calculated by applying Eq.s (1) and (2):

$$\boldsymbol{RNOc}(\%) = \frac{\boldsymbol{A_f}}{\boldsymbol{A_i}} \times 100 \quad (1)$$

$$\boldsymbol{ROSp}(\%) = 100 - \boldsymbol{RNOc} \quad (2)$$

RNOc is the percentage of RNO consumed, A_i is the initial absorption of the RNO, A_f is the final absorption of the RNO, and ROSp is the ROS produced percentage. The measurements were performed in triplicate.

2.7. Microorganism

The *S. aureus* strain used in this study was isolated by Medeiros et al. (2011) [35]. The strain was reactivated in nutrient broth in a bacteriological oven (37 ± 2.5 °C) for 24 h. The working microorganism concentration was established as 10^8 $CFU \cdot mL^{-1}$ by setting the optical density to 0.08−0.1 using a spectrophotometer at a wavelength of 595 nm.

2.8. Cytotoxicity study of AgNPrs

The cytotoxicity of AgNPrs was evaluated using the MTT method (3-(4,5-dimethylthiazol-2-yl)-2,5-diphenyltetrazolium Bromide) [40] on JJ74.A1 (macrophages, BCRJ – Rio de Janeiro Cell Bank, 0121) cell line. The cells were grown in DMEM (Dulbecco's Modified Eagle's Medium) supplemented with fetal bovine serum (10 %) and penicillin-streptomycin (1%) in an incubator at 37 °C in a humid

atmosphere enriched with 5% CO_2. Cells (1×10^4 cells/mL) were distributed in 96-well plates and incubated for 24 h. For this experiment, five concentrations of AgNPrs were tested (0, 0.01, 0.1, 1 e 10 $\mu g \cdot mL^{-1}$). After 24 h of incubation, 20 μL of MTT (4 mg/mL) was added to each system, and after 3 h of incubation, the supernatant was aspirated, and 100 μL of DMSO (Dimethyl sulfoxide) was added to each well. The absorbance was measured in a microplate reader (Elx808 Biotek) at a wavelength of 630 nm. The experiments were carried out in triplicate. The results were expressed in cell viability: (A_{630} of the treated cell population × 100 / A_{630} of the untreated cell population) [41].

2.9. Photodynamic study on S. aureus

The same light system of section 2.6 was used to study the photodynamic action on *S. aureus*. The irradiance used was 45.8 $mW \cdot cm^{-2}$, with radiant exposure of *ca.* 8.0; 16.0, and 24.0 $J \cdot cm^{-2}$, corresponding to 3, 6, and 9 min of irradiation, respectively. The irradiation was carried out in a 96-well plate, which was inserted into the chamber without a lid.

The inoculum was diluted to a final concentration of 10^5 $CFU \cdot mL^{-1}$ using PBS. The groups were divided into (i) control, which received no light or treatment, (ii) irradiated group, treated only LED light, and (iii) groups that received treatment with MB or AgNPr-MB (both with a photosensitizer concentration of 45 $\mu mol \cdot L^{-1}$). Groups incubated with only MB, AgNPrs, or AgNPr-MB without irradiation (under dark conditions) were also tested to evaluate any antibacterial activity associated with those systems. Positive control was performed using 0.12 % chlorhexidine. The pre-incubation time was 10 min using a shaker (50 rpm). After treatment, the bacteria were diluted to a final concentration of 10^4 $CFU \cdot mL^{-1}$, and then 100 μL were added on a plate with Mueller-Hinton agar and plated using a shaped handle. The plates were kept in a bacteriological oven (37 ± 2.5 °C) for 24 h. The colonies were then counted and expressed as $CFU \cdot mL^{-1}$. All the experiments were performed in triplicate.

2.10. Statistical analysis

The cytotoxic analysis results were expressed as a mean ± SD, $p < 0.05$ and were submitted to ANOVA followed by Bonferroni using the GraphPad Prisma 7.0 program. For the inactivation analysis, the results were expressed as mean ± SD, $p < 0.05$, and ANOVA statistics followed by Tukey test were performed using GraphPad Prisma 7.0 program.

3. Results

3.1. Characterization of Ag NPs

Aiming at photodynamic applications enhanced by FRET mechanisms, it is fundamental to apply metallic particles with a plasmon band overlapping the absorption region of the photosensitizer. As the LSPR for AgNPrs is dependent on their size/thickness [42], we have grown three different sets of particles from the Ag seeds. Fig. 2(a) shows the extinction spectra of AgNPrs we prepared in this study. The Ag particles used as seeds for the prismatic growth show the characteristic plasmonic band at 400 nm (full width at half maximum, FWHM = 85 nm). For all the other systems we distinctively observe two plasmon bands: a transversal one that corresponds to the spherical residual NPs still present at $\lambda \sim 400$ nm (bold arrow on the plot, Fig. 2a), and a longitudinal band that indicates the presence of prismatic shape NPs [36] at different spectral regions indicating different particle size distributions. The first set of nanoprisms show an extinction maximum at 488 nm (FWHM = 85 nm), the second set shows a maximum at $\lambda = 545$ nm (FWHM = 113 nm), and the third set presents a maximum at $\lambda = 621$ nm (FMHW = 168 nm).

Fig. 2b shows the absorption spectra of MB and AgNPr3, displaying a significant spectral overlap of both systems. For that reason, these particles were chosen to test our hypothesis of plasmonic PDI enhancement.

HRTEM images of Ag seeds and conventional TEM images of AgNPr3 systems were used to access the particles' morphological characteristics, Fig. 3(a–c). Three distinct morphologies may be observed: prismatic nanoplatelets, spherical and less frequent, truncated prisms. Dong et *al* (2012) [43], using the reduction synthesis method, observed the same morphological pattern, and they attributed the difference in size and shapes of the AgNPrs to the increase of reaction time, which enabled a differentiation in the particle growth. In our results, two relevant populations, seeds and the particles grown from them, describe the average dimensions of our Ag NP systems, and the size distribution can be observed in Fig. 3(d). Taking the spherical particles' diameter, we obtain a size average of $d = 12 \pm 6$ nm, and taking a longitudinal length of the prisms and truncated prisms we observe an average size of $d = 32 \pm 6$ nm.

DRX measurements of AgNPrs dispersed in PVA films showed characteristic $2\theta = 38.1$; 64.5 and 77.5 corresponding, respectively, to the (111), (220) and (311) reflections of the silver face-centered cubic crystal phase (JCPDS No: 04-0783) [44, 45] (Fig. 4a). The PVA diffraction profile observed shows a reflection at $2\theta = 40.6$, which is

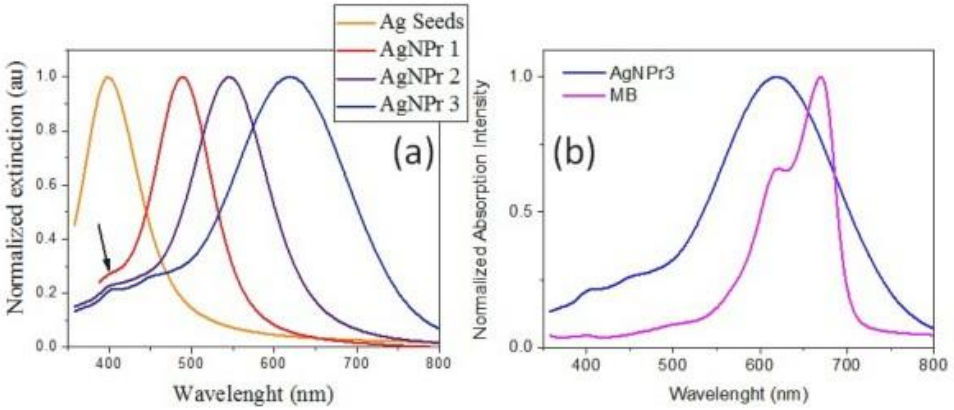

Fig. 2. (a)Extinction spectra of Ag seeds (orange) applying PSSS as the surfactant in the synthesis. Red, purple, and blue lines are longitudinal plasmon bands of the nanoprisms obtained by adding different amounts of the seed volume to the reaction medium: AgNPr1 (650 μL), AgNPr2 (400 μL), and AgNPr3 (200 μL) and (b) Extinction spectra of AgNPr3 and MB used to conjugation.

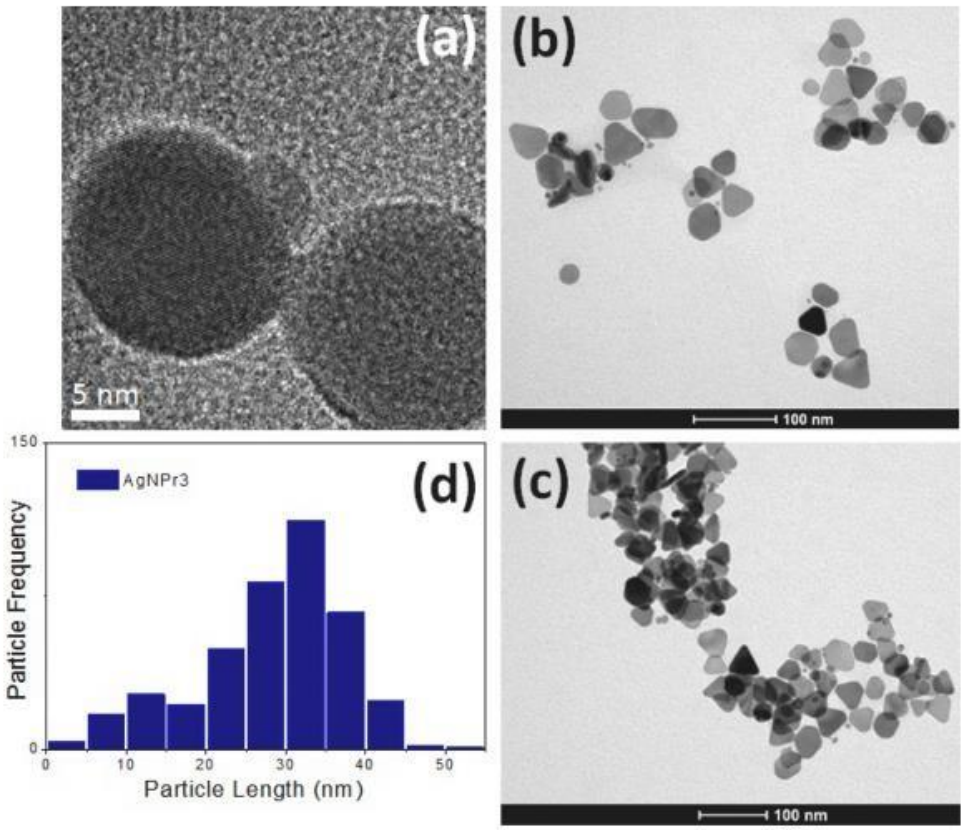

Fig. 3. TEM images of Ag NPs prepared using PSSS. (a) HRTEM image of Ag seeds; (b) and (c) TEM images of grown AgNPr3 particles. (d) The size distribution of the AgNPr3 particles.

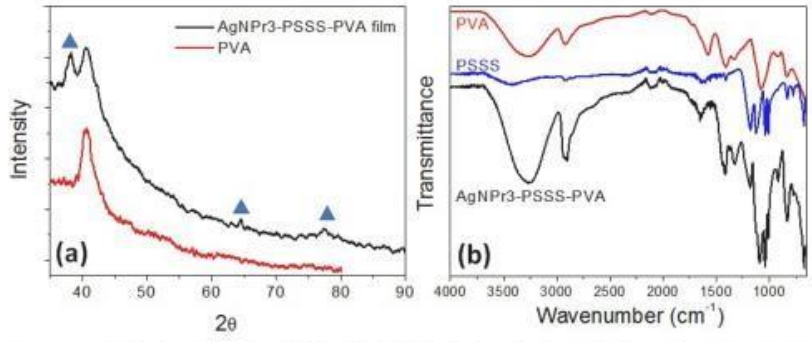

Fig. 4. (a) X-ray Diffraction pattern of AgNPr3 particles embedded in a 1% PVA film, showing the characteristic reflections of Ag FCC phase (blue triangles). PVA DRX is also depicted. (b) Infrared absorption vibrational spectra of PVA, PSSS and of the AgNPr3-PSSS embedded in the PVA film.

very characteristic for PVA films and powder [46]. FTIR spectral profile of the AgNPr3–PSSS particles embedded in the PVA film is depicted in Fig. 4(b). We observed that some of the characteristic infrared absorption frequencies of PSSS and PVA show spectral overlap, especially those in the 4000 – 1570 cm^{-1} range, corresponding to symmetric and/or asymmetric stretching frequencies of –OH, $-CH_2$, and –CH, present in both, PSSS and PVA molecular structures. Nevertheless, characteristic PSSS frequencies were able to be assigned although, also overlapped to PVA absorption frequencies. The band at ν =674 $cm^{-1}$is characteristic of the out-of-plane skeleton bending vibrations of benzene ring while the band, which refers to the out-of-plane bending vibration of the —CH groups in the benzene ring, is found at —ν =774 cm^{-1}. The band at ν =833 cm^{-1}, corresponds to the *para* substitution of the ring [47] and is overlapped to the PVA CC— stretching band [48]. The frequencies observed at ν = 1004 and 1035 cm^{-1}, respectively, refer to the in-plane bending vibration and the in-plane skeleton vibration of benzene ring

[49], while the peaks at ν = 1115 and 1171 cm^{-1} correspond to the symmetric and antisymmetric vibration frequencies of $-SO_3^-$ groups of the PSSS molecule [49]. We observe in the spectrum of AgNPr3-PSSS-PVA presented in Fig. 4(b) that all these PSSS characteristic bands are overlapped to the stretching of —CO and the bending of OH PVA groups (=—ν =1081 cm^{-1}). Moreover, the following observed bands refer to PVA functional groups: ν =1328 cm^{-1} bending of O—H and wagging of CH; ν =1643 cm^{-1} stretching of CO group and —=ν =1416 cm^{-1}, which corresponds to C—H_2 bending.

Analyzing the width of the nanoprisms by TEM images, we observed an average of w = 6.6 ± 2 nm and applied these dimensions to simulate their plasmonic field enhancement. The simulated extinction maxima for four different sizes of prismatic nanoplatelets (d = 20, 25, 32.5, and 39.5 nm) with a 6.6 nm width is shown in Fig. 5(a). These spectral maxima agree to the AgNPr3 extinction spectral profiles (Fig. 2a), considering the broad size distribution observed and the residual presence of small quantities of nanospheres. Fig. 5(b) displays the normalized electric field distribution (|E / E0|) simulated around a single silver nanoprism at λ_0 = 630 nm with d = 35.5 nm and thickness = 6.6 nm, in free space. As we observe, the field enhancement is highly localized at the tips of silver nanoprism. In this case, a field enhancement 30 times higher as compared to the incident field was achieved.

3.2. Characterization of AgNPr-MB conjugates

The association of AgNPr3 and MB was carried out by electrostatic interactions between the negatively charged AgNPr3-PSSS and the positive MB species. Macroscopically, the AgNPr–MB systems' preparation showed no signs of colloidal instability, and the systems presented no signs of color change or precipitation. Fig. 6(a) shows the UV–vis electronic spectra of MB and the resulting conjugated system AgNPr3–MB shows no difference in the MB absorption profile in the presence of NPs. There was a small decrease in the weakest MB band (~ 605 nm), which corresponds to MB—MB dimer formation, and we suggest that MB interaction with the nanoprisms decreases MB dimerization process. The emission spectrum of the AgNPr3–MB conjugates (Fig. 6b) shows a 6 nm spectral shift, towards a higher wavelength, indicating a change in the MB species' electronic environment and suggesting interaction between the nanoprisms and the photosensitizer molecules [50].

The AgNPr3–MB interaction was also corroborated by measuring the ζ changes of the original AgNPr3 after their incubation with cationic MB molecules. For the initial Ag seeds, a negative value was obtained (ζ = -7.1 ± 0.6 mV), and a much lower value for the AgNPr3 systems (ζ = -42.9 ± 0.3 mV), which can be explained by the presence of PSSS molecules attached to the surface of the particles [36]. For the AgNPr3–MB system, ζ value was about 2-fold smaller (-20 ± 0.7 mV), indicating the electrostatic interaction of MB molecules with the nanoprisms.

3.3. In vitro ROS generation

The results for the ROS generation are depicted in Table 1 for two different irradiation conditions. The continuous irradiation of 60 s was more effective compared to the irradiation time-frequency of 20 s. However, at both irradiation times, AgNPr3–MB nanoconjugates induced a more significant degradation of the RNO, generating a 15 % higher ROS production than the MB alone.

3.4. Cytotoxicity study

Results showed that the three AgNPr systems used in our study did not lead to significant cytotoxicity on J774A.1 cells, presenting cell viability above 90 % after 24 h incubation (Fig. 7).

To determine whether the samples' antibacterial activity was induced solely by photodynamic activity, we monitored the *S. aureus* bacterial viability applying AgNPr3, and AgNPr3–MB conjugates, under dark condition. Fig. 8 shows a slight decrease in bacterial viability (less than 1 log) associated with the AgNPr3 system itself. This was expected since the antibacterial property of Ag NPs has already been reported [51–53]. AgNPr3–MB also showed a small effect on the bacterial viability, but even less pronounced than the bare particles. We suggest that the MB molecules associated with the particles interfere in their antibacterial action, probably by either decreasing their physical contact with the cells or by decreasing the decomposition of the Ag NPs, thus decreasing the Ag^+ *in situ* formation, one of the effective pathways described in the literature of the lethal action of Ag NPs [51]. Moreover, MB itself in low concentrations has many good antioxidant properties and may act as an electron acceptor in the electron transport chain in mitochondria, enhancing cell ATP production [54].

3.5. Photodynamic inactivation of S. aureus isolated from buffalo mastitis

No substantial effect of MB in the dark or only upon exposure to red light without MB was observed for the bacteria's viability in all experiments (Fig. 9). In experiments containing MB at 45 μmol·L^{-1}, a reduction (1 log) was observed after 9 min of irradiation, but there was no complete inactivation of the strain. In all studies, 0.12 % chlorhexidine achieved complete inactivation (under dark conditions), with no detected bacterial growth.

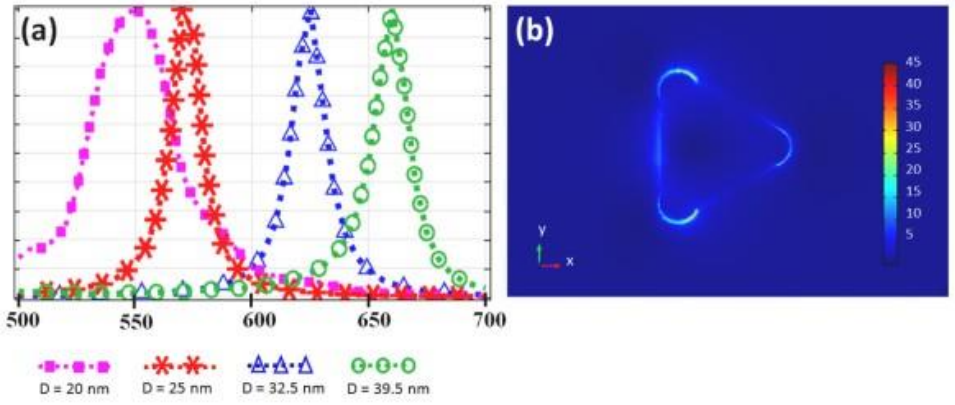

Fig. 5. (a) Simulated plasmon bands for Ag prismatic nanoplatelets ranging from d = 20 to 39.5 nm (considering 6.6 nm thickness) in water. (b) Electric field enhancement for a prismatic nanoplatelet of d = 35.5 nm (6.6 nm thickness) placed in free space.

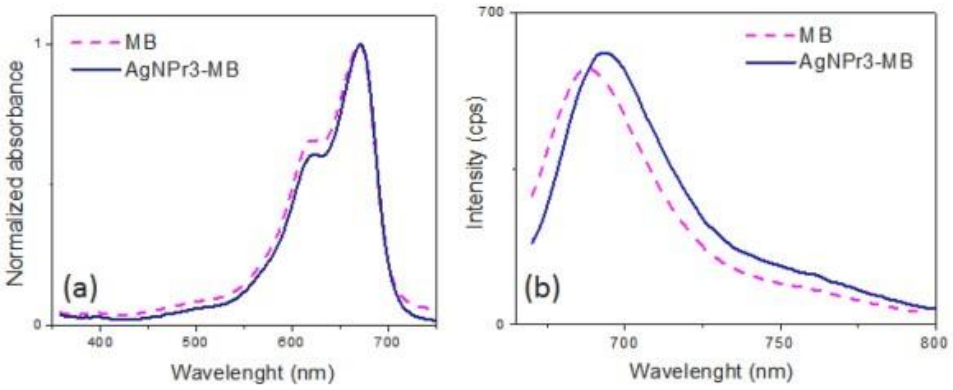

Fig. 6. Absorption (a) and emission (b, λ_{exc} = 660 nm) spectra of MB species and AgNPr3-MB conjugates.

Table 1
ROS (%) generated by AgNPr3, MB, and AgNPr3-MB after a total of 300 s of irradiation. We applied two irradiation conditions: 20 s or 60 s periods. MB and AgNPr3-MB were kept at the same concentration (15 μmol·L^{-1}).

System	ROS (%) after 300 s irradiation	
	20 s	60 s
AgNPr3	5.9 ± 1.7	9.9 ± 2.7
MB	60.5 ± 1.2	77.4 ± 1.9
AgNPr3–MB	72.3 ± 0.3	89.7 ± 0.6

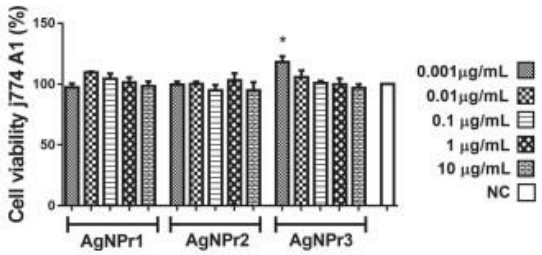

Fig. 7. Cell viability of J774A.1 macrophages after incubation with Ag nanoprisms (AgNPr) of three different sizes. *p < 0.05 *vs.* Control. Each value determines the mean ± SD of three independent experiments. NC: negative control.

4. Discussion

The nanoprisms preparation can be divided into two stages, the first being the nucleation of Ag_n by reducing Ag^+ ions with $NaBH_4$, a potent reduction agent, forming spherical seeds. By analyzing TEM images, we observe that our Ag seeds show a size distribution of d = 12 ± 6 nm. Assuming the total reduction of 0.5 mmol Ag ions to form monodisperse 12 nm size seeds, we estimate a total amount of 10^{14} NPs/mL, which is a rough estimate, considering a 50 % size dispersion. These seeds were stabilized through the interaction of the PSSS surfactant polymer to specific crystallographic planes at the particles' surface [36]. In the second stage, we induced their further growth by adding more Ag^+ ions. The PSSS species induced the seeds' anisotropic growth, generating prismatic NPs [36,55] (as schematized in Fig. 1). DRX measurements show the expected reflections for the FCC Ag crystal structures for the AgNPr3 systems (Fig. 4a) and FT-IR analysis confirmed the presence of PSSS (Fig. 4b) on the final grown particles. We applied here the methodology of Aherne and coll. (2008) by inducing further growth of

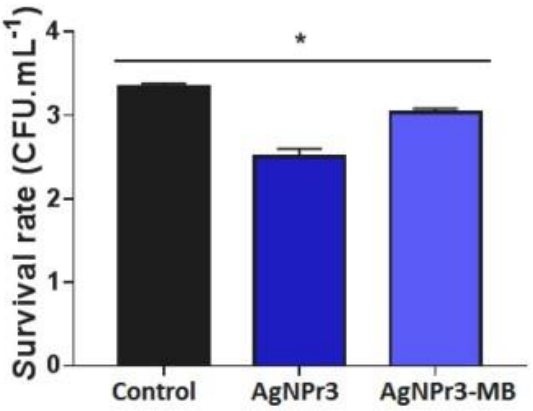

Fig. 8. Cytotoxicity assay on *S. aureus* strain applying AgNPr3 and AgNPr3-MB conjugates under dark conditions, without irradiation. *, p < 005 *vs.* Control.

different initial seed volumes, we obtained nanoprisms (also referred to as prismatic nanoplatelets) with three distinct plasmon bands peaking at λ = 488, 544, and 619 nm, as shown in Fig. 2a. We applied the AgNPr3 sample, which presented a very good spectral overlap with the electronic absorption profile of MB (Fig. 2b), aiming at the plasmonic enhancement of this photosensitizer. We also simulated the plasmonic field enhancement of 24–39.5 nm size nanoprisms. Applying the average thickness of the AgNPr3 particles (6.6 nm), we observed an excellent correlation between the nanoprisms plasmon band wavelengths of the simulations and those observed experimentally. As expected, the field enhancement is highly localized at the tips of Ag prismatic nanoplatelets. The particles' simulation in free space shows a field enhancement 30 times higher than the incident field. Sherry and coll. [56] applying electrodynamic modeling based on the discrete dipole approximation demonstrated that the plasmonic properties of single Ag nanoprisms are highly related to their thickness, showing that as a key role in their plasmonic enhancement. The images show very thin nanoprisms (lateral length ~6 times wider than the thickness), rendering a great residual area for MB attachment in the flat sides where the PSSS is associated.

The AgNPr3-MB system showed a ζ value about 2-fold smaller (*ca.* – 20 mV) than AgNPr3 (*ca.* - 43 mV). This result, along with the spectral shift observed for the original MB fluorescence profile (Fig. 4b), strongly suggests that we were successfully obtained conjugates. Yamamoto et al.

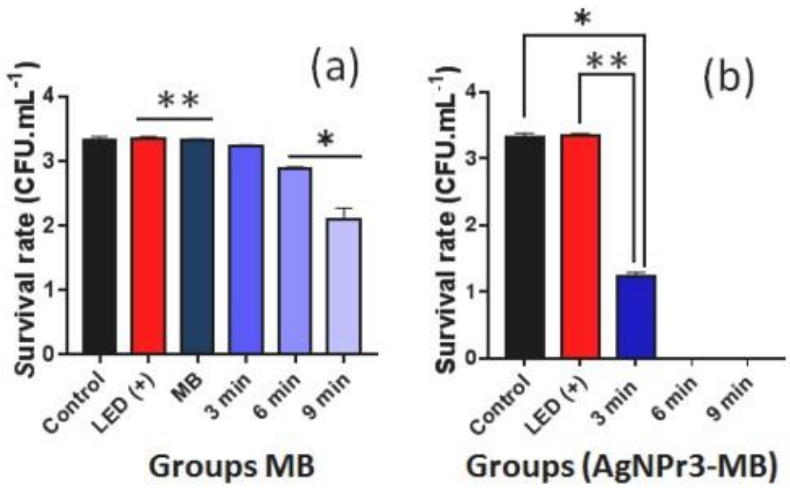

Fig. 9. Evaluation of *S. aureus* inactivation under irradiation with red light (45.8 mW·cm^{-2} of irradiance) of (A) MB groups (Control, LED (+), only MB and three irradiation times: 3, 6 and 9 min; n = 3, mean ± SD) *, $p < 0.05$ *vs.* Control; **, $p < 0.05$ *vs.* LED irradiation for 6 min and (B) when treated with MB-NPs nanosystems and irradiated for 3, 6, and 9 min under red light (45.8 mW ·cm^{-2} of irradiance) *, $p < 005$ *vs.* Control; **, $p < 005$ *vs.* LED (+) for 3 min.

(2018) also used electrostatic interactions to associate Au NPs coated with serum bovine albumin to MB molecules [57], showing a perfect interaction. Misba et al. [58] associated spherical AgNPs and the orto-toluidine blue (TBO) PS by electrostatic interaction, exploring the negative charge of citrate coated Ag NPs and the positive charge of the amine group of TBO. In their work, they corroborated their studies with the work of Bryaskova et al. [59], who used AgNPs stabilized with polyvinylpyrrolidone (PVP). They showed more excellent stability and reactivity of the particles due to the interaction with the polymer.

Up to the present study, there are no reports in the literature on the use of photodynamic treatment using metallic nanoparticles conjugated to PS to inactivate isolated strains of buffalo mastitis. However, several alternative approaches have already been reported, such as the use of homeopathy together with extracts and antibiotics [60,61] and the use of PDT to inactivate bovine mastitis *in vitro* [62] and *in vivo* [63]. Sellera et al. using MB and red light (100 mW/cm^2) irradiation for 3 min, inactivated several bacteria (*Streptococcus agalactiae*, *Streptococcus dys-galactiae*, *Staphylococcus aureus*, and *Corynebacterium bovis*) presented in bovine mastitis using a working concentration of 50 μmol·L^{-1} [62]. In another work, Moreia et al. tested photoinactivation in cows with mastitis, using toluidine blue as PS and red light irradiation (20 mW/cm^2). The results showed this technique's potential to be used *in vivo* for overcoming antibiotic treatment [63]. Comparing the use of MB with and without Ag NPs, we observe that their association increased the photodynamic inactivation efficiency. First of all, we observed a 15 % increase in ROS production of the AgNPr3-MB conjugates compared to the MB alone. We believe that this is due to the plasmonic enhancement enabled by the Ag prismatic nanoplatelets. The AgNPr3s alone showed a 9.9 ± 2.7 % ROS production after 5 min irradiation. We suggest that may result from localized charging of the Ag nanoprisms and subsequent discharge, reacting with dissolved oxygen [64]. After coating these particles with MB species, we firmly believe that the enhancement of the reactive species production is due to the surface plasmon resonance effect due to FRET [33] mechanism. Yamamoto et al. [57] observed that the association of MB with Au NPs, also showed a higher production of singlet oxygen when compared to the PS alone. This was also observed by Misba et al. [58] using the PS TBO. They observed a higher intracellular production of ROS when TBO–AgNPs conjugates were used, compared to only TBO species. In both studies, the authors suggest that energy transfer occurred from the NPs to the PS through surface plasmon resonance. Thus, our findings are corroborating other works presented in the literature.

Applying MB for photoinactivation of *S. aureus*, we observe a decrease in bacterial viability, highly dependent on the radiant exposure of light used. However, it was impossible to observe total inactivation in any of the tested times, which shows that a longer irradiation time should inactivate the strain under study. Vilela et al. [65] studied the inactivation of isolated clinical strains of *S. aureus*. They observed that applying MB at 300 μmol.L^{-1} with a red light irradiation time of 5 min (100 mW/cm^2) reduced just 1 bacterial log. The literature already reports the absence of dark toxicity for MB, showing that it can be used up to a dose of 3.292 μM in humans [66]. Several PDT treatment studies *in vivo*, using MB, have already been reported, such as dermatoses in sheep [67] and gingivostomatitis in dogs [68]. *In vitro*, there are also reports of inactivation of *Trichomonas vaginalis* [16], *Streptococcus mutans* [69], and *Candida albicans* [70]. The MB concentration used in our experiment, as well as the irradiance used, was lower than the values already reported in the literature, applying MB as photosensitizers.

In contrast, when applying the AgNPr3–MB systems, we observed a bacterial reduction (less than 1 log) after incubation for 24 h under dark conditions. On the other hand, our PDI studies applying AgNPr–MB conjugates showed that after 3 min irradiation, a 2 log bacterial reduction could be reached, compared to the control group. Furthermore, in the treatment of *S. aureus* applying the conjugates and 6 min irradiation, a total inactivation was achieved (Fig. 9). At the same time, less than 0.5 log reduction was obtained using only MB, showing the effectiveness of the association of MB and AgNPr3 for bacteria inactivation. It is worth mentioning that studies that reduce the concentration of the photosensitizer and/or the irradiation time are extremely promising to improve the photodynamic treatment.

The synergistic effect of metal nanoparticles and photosensitizers has already been addressed in the literature, as shown above. Many studies show that spherical Ag NPs, for instance, act synergistically with PS in photodynamic-related processes [27,71]. One assumption is that the conjugation between PS and metallic nanoplatforms would promote more significant adsorption to the bacterial wall. By connecting to the external membrane, the production of ROS would be more localized [52]. We strongly believe that the MB absorption band's spectral tuning with the AgNPrs plasmon band favored the amplification of the photodynamic action. As described previously, Ag NPs, due to their

antimicrobial activity, has been associated with several PSs and used for bacterial PDI studies, but this is the first time Ag nanoprisms were applied to improve the photodynamic action profiting of their increased LSPR phenomena, not only decreasing the working MB concentration but also by decreasing the total irradiation dose. These results showed the potential of this therapy to be used *in vivo* on inactivation of several mastitis strains and other bacteria.

5. Conclusion

In this work, we showed that the association of Ag prismatic nanoplatelets with MB increased the PDI process's effectiveness, and we strongly suggest that this resulted from the plasmonic FRET process. AgNPr3–MB can be a good system for the photodynamic treatment of mastitis. We believe that this therapy strategy should replace the use of antibiotics and that we expect it to be effective even for bacterial resistance cases. Moreover, Ag nanoprisms show intensified plasmonic properties related to their shape and size. These systems' ability to be optically tunable may potentialize their application to several photosensitizers active in the visible, showing a great versatility aspect for FRET plasmon-induced PDI.

Acknowledgments

The authors are grateful to Conselho Nacional de Desenvolvimento Científico e Tecnológico (CNPq, Grant Nr. 424235/2018-8), Coordenação de Aperfeiçoamento de Pessoal de Nível Superior (CAPES), and FACEPE (Fundação de Amparo à Ciência e Tecnologia do Estado de Pernambuco, Grant Nr. APQ-0573-2.09/18 and BFP-0079-5.05/20). This work was also funded by INCT of Photonics and by Associated Nanotechnology Laboratories (LARNano/UFPE). We would like to thank Fundação Oswaldo Cruz (FIOCRUZ) for the transmission electron microscopy images. We are especially grateful to Prof E. Padron of the Physics Department of UFPE for XRD analysis and Prof. C. Sampaio of the Laboratório de Biofísica Química of the UFPE for FTIR measurements, during the COVID 19 pandemic state.

References

[1] F. Gomes, M. Henriques, Control of bovine mastitis: old and recent therapeutic approaches, Curr. Microbiol. 72 (2016) 377–382, https://doi.org/10.1007/s00284-015-0958-8.

[2] A.-M. Heikkilä, E. Liski, S. Pyörälä, S. Taponen, Pathogen-specific production losses in bovine mastitis, J. Dairy Sci. 101 (2018) 9493–9504, https://doi.org/10.3168/jds.2018-14824.

[3] J. Barlow, Mastitis Therapy and Antimicrobial Susceptibility: a Multispecies Review with a Focus on Antibiotic Treatment of Mastitis in Dairy Cattle, J. Mammary Gland Biol. Neoplasia 16 (2011) 383–407, https://doi.org/10.1007/s10911-011-9235-z.

[4] C. Catozzi, A. Sanchez Bonastre, O. Francino, C. Lecchi, E. De Carlo, D. Vecchio, A. Martucciello, P. Fraulo, V. Bronzo, A. Cuscó, S. D'Andreano, F. Ceciliani, The microbiota of water buffalo milk during mastitis, PLoS One 12 (2017) e0184710, https://doi.org/10.1371/journal.pone.0184710.

[5] K. Hughes, C.J. Watson, The mammary microenvironment in mastitis in humans, dairy ruminants, rabbits and rodents: a one health focus, J. Mammary Gland Biol. Neoplasia 23 (2018) 27–41, https://doi.org/10.1007/s10911-018-9395-1.

[6] H. Abrahamse, M.R. Hamblin, New photosensitizers for photodynamic therapy, Biochem. J. 473 (2016) 347–364, https://doi.org/10.1042/BJ20150942.

[7] B. Li, L. Lin, H. Lin, B.C. Wilson, Photosensitized singlet oxygen generation and detection: recent advances and future perspectives in cancer photodynamic therapy, J. Biophotonics 9 (2016) 1314–1325, https://doi.org/10.1002/jbio.201600055.

[8] M.R. Hamblin, H. Abrahamse, Can light-based approaches overcome antimicrobial resistance? Drug Dev. Res. 80 (2019) 48–67, https://doi.org/10.1002/ddr.21453.

[9] S. Kwiatkowski, B. Knap, D. Przystupski, J. Saczko, E. Kędzierska, K. Knap-Czop, J. Kotlińska, O. Michel, K. Kotowski, J. Kulbacka, Photodynamic therapy - mechanisms, photosensitizers and combinations, Biomed. Pharmacother. 106 (2018) 1098–1107, https://doi.org/10.1016/j.biopha.2018.07.049.

[10] M.R. Hamblin, Antimicrobial photodynamic inactivation: a bright new technique to kill resistant microbes, Curr. Opin. Microbiol. 33 (2016) 67–73, https://doi.org/10.1016/j.mib.2016.06.008.

[11] A.F. Silva, A. Borges, E. Giaouris, J.M. Graton Mikcha, M. Simões, Photodynamic inactivation as an emergent strategy against foodborne pathogenic bacteria in planktonic and sessile states, Crit. Rev. Microbiol. 44 (2018) 667–684, https://doi.org/10.1080/1040841X.2018.1491528.

[12] J. Zhuang, H. Yang, Y. Li, B. Wang, N. Li, N. Zhao, Efficient photosensitizers with aggregation-induced emission characteristics for lysosome- and Gram-positive bacteria-targeted photodynamic therapy, Chem. Commun. 56 (2020) 2630–2633, https://doi.org/10.1039/D0CC00394H.

[13] F. Halili, A. Arboleda, H. Durkee, M. Taneja, D. Miller, K.A. Alawa, M.C. Aguilar, G. Amescua, H.W. Flynn, J.-M. Parel, Rose bengal– and riboflavin-mediated photodynamic therapy to inhibit methicillin-resistant Staphylococcus aureus keratitis isolates, Am. J. Ophthalmol. 166 (2016) 194–202, https://doi.org/10.1016/j.ajo.2016.03.014.

[14] J. Tan, Z. Liu, Y. Sun, L. Yang, L. Gao, Inhibitory effects of photodynamic inactivation on planktonic cells and biofilms of Candida auris, Mycopathologia 184 (2019) 525–531, https://doi.org/10.1007/s11046-019-00352-9.

[15] J.D. Martinez, A. Naranjo, G. Amescua, S.R. Dubovy, A. Arboleda, H. Durkee, M. C. Aguilar, H.W. Flynn, D. Miller, J.-M. Parel, Human corneal changes after rose bengal photodynamic antimicrobial therapy for treatment of fungal keratitis, Cornea 37 (2018) e46–e48, https://doi.org/10.1097/ICO.0000000000001701.

[16] T.H. Silva Fonseca, M. Alacoque, F.M. Silva Oliveira, B.M. Soares, H.V. Leite, M. V. Caliari, M.A. Gomes, H. Busatti, Photodynamic therapy as a new approach to Trichomonas vaginalis inactivation, Photodiagnosis Photodyn. Ther. 22 (2018) 91–95, https://doi.org/10.1016/j.pdpdt.2018.02.006.

[17] C.G. Andrade, R.C.B.Q. Figueiredo, K.R.C. Ribeiro, L.I.O. Souza, J.F. Sarmento-Neto, J.S. Rebouças, B.S. Santos, M.S. Ribeiro, L.B. Carvalho, A. Fontes, Photodynamic effect of zinc porphyrin on the promastigote and amastigote forms of Leishmania braziliensis, Photochem. Photobiol. Sci. 17 (2018) 482–490, https://doi.org/10.1039/C7PP00458C.

[18] A.U. Khan, Q. Yuan, Y. Wei, S.U. Khan, K. Tahir, Z.U.H. Khan, A. Ahmad, F. Ali, S. Ali, S. Nazir, Longan fruit juice mediated synthesis of uniformly dispersed spherical AuNPs: cytotoxicity against human breast cancer cell line MCF-7, antioxidant and fluorescent properties, RSC Adv. 6 (2016) 23775–23782, https://doi.org/10.1039/C5RA27100B.

[19] A.J. Haes, R.P. Van Duyne, A nanoscale optical biosensor: sensitivity and selectivity of an approach based on the localized surface plasmon resonance spectroscopy of triangular silver nanoparticles, J. Am. Chem. Soc. 124 (2002) 10596–10604, https://doi.org/10.1021/ja020393x.

[20] A.U. Khan, Q. Yuan, Y. Wei, G.M. Khan, Z.U.H. Khan, S. Khan, F. Ali, K. Tahir, A. Ahmad, F.U. Khan, Photocatalytic and antibacterial response of biosynthesized gold nanoparticles, J. Photochem. Photobiol. B, Biol. 162 (2016) 273–277, https://doi.org/10.1016/j.jphotobiol.2016.06.055.

[21] L.S.A. de Melo, C.R. Chaves, P.E.C. Filho, S. Saska, K. Nigoghossian, A.S.L. Gomes, Y. Messaddeq, S.J.L. Ribeiro, B.S. Santos, A. Fontes, R.E. de Araujo, Luminescence enhancement of carboxyl-coated CdTe quantum dots by silver nanoparticles, Plasmonics 8 (2013) 1147–1153, https://doi.org/10.1007/s11468-013-9524-z.

[22] M. Rycenga, C.M. Cobley, J. Zeng, W. Li, C.H. Moran, Q. Zhang, D. Qin, Y. Xia, Controlling the synthesis and assembly of silver nanostructures for plasmonic applications, Chem. Rev. 111 (2011) 3669–3712, https://doi.org/10.1021/cr100275d.

[23] K. Shitomi, H. Miyaji, S. Miyata, T. Sugaya, N. Ushijima, T. Akasaka, H. Kawasaki, Photodynamic inactivation of oral bacteria with silver nanoclusters/rose bengal nanocomposite, Photodiagnosis Photodyn. Ther. 30 (2020) 101647, https://doi.org/10.1016/j.pdpdt.2019.101647.

[24] L.S.A. de Melo, A.S.L. Gomes, S. Saska, K. Nigoghossian, Y. Messaddeq, S.J. L. Ribeiro, R.E. de Araujo, Singlet oxygen generation enhanced by silver-pectin nanoparticles, J. Fluoresc. 22 (2012) 1633–1638, https://doi.org/10.1007/s10895-012-1107-4.

[25] M.S. Ribeiro, L.S.A. de Melo, S. Farooq, A. Baptista, I.T. Kato, S.C. Núñez, R.E. de Araujo, Photodynamic inactivation assisted by localized surface plasmon resonance of silver nanoparticles: in vitro evaluation on Escherichia coli and Streptococcus mutans, Photodiagnosis Photodyn. Ther. 22 (2018) 191–196, https://doi.org/10.1016/j.pdpdt.2018.04.007.

[26] S.M. Shabangu, B. Babu, R.C. Soy, J. Oyim, E. Amuhaya, T. Nyokong, Susceptibility of Staphylococcus aureus to porphyrin-silver nanoparticle mediated photodynamic antimicrobial chemotherapy, J. Lumin. 222 (2020) 117158, https://doi.org/10.1016/j.jlumin.2020.117158.

[27] P.G. Mahajan, N.C. Dige, B.D. Vanjare, S.-H. Eo, S.-Y. Seo, S.J. Kim, S.-K. Hong, C.-S. Choi, K.H. Lee, A potential mediator for photodynamic therapy based on silver nanoparticles functionalized with porphyrin, J. Photochem. Photobiol. A: Chem. 377 (2019) 26–35, https://doi.org/10.1016/j.jphotochem.2019.03.034.

[28] V.P.S. Jesus, L. Raniero, G.M. Lemes, T.T. Bhattacharjee, P.C. Caetano Júnior, M. L. Castilho, Nanoparticles of methylene blue enhance photodynamic therapy, Photodiagnosis Photodyn. Ther. 23 (2018) 212–217, https://doi.org/10.1016/j.pdpdt.2018.06.011.

[29] P. Khoza, I. Ndhundhuma, A. Karsten, T. Nyokong, Photodynamic therapy activity of phthalocyanine-silver nanoparticles on melanoma Cancer cells, J. Nanosci. Nanotechnol. 20 (2020) 3097–3104, https://doi.org/10.1166/jnn.2020.17398.

[30] A.U. Khan, Q. Yuan, Y. Wei, Zul H. Khan, K. Tahir, S.U. Khan, A. Ahmad, S. Khan, S. Nazir, F.U. Khan, Ultra-efficient photocatalytic deprivation of methylene blue and biological activities of biogenic silver nanoparticles, J. Photochem. Photobiol. B, Biol. 159 (2016) 49–58, https://doi.org/10.1016/j.jphotobiol.2016.03.017.

[31] A.U. Khan, A. ur Rahman, Q. Yuan, A. Ahmad, Z.U.H. Khan, M.H. Mahnashi, B. A. Alyami, Y.S. Alqahtani, S. Ullah, A.P. Wirman, Facile and eco-benign fabrication of Ag/Fe2O3 nanocomposite using Algaia Monozyga leaves extract and its' efficient biocidal and photocatalytic applications, Photodiagnosis Photodyn. Ther. 32 (2020) 101970, https://doi.org/10.1016/j.pdpdt.2020.101970.

[32] A.U. Khan, A.U. Khan, B. Li, M.H. Mahnashi, B.A. Alyami, Y.S. Alqahtani, A. O. Alqarni, Z.U.H. Khan, S. Ullah, M. Wasim, Q.U. Khan, W. Ahmad, Biosynthesis of silver capped magnesium oxide nanocomposite using Olea cuspidata leaf extract and their photocatalytic, antioxidant and antibacterial activity, Photodiagnosis Photodyn. Ther. 33 (2021) 102153, https://doi.org/10.1016/j.pdpdt.2020.102153.

[33] J. Zhang, Y. Fu, J.R. Lakowicz, Enhanced förster resonance energy transfer (FRET) on a single metal particle, J. Phys. Chem. C. 111 (2007) 50–56, https://doi.org/10.1021/jp062665e.

[34] J.P. Tardivo, A. Del Giglio, C.S. de Oliveira, D.S. Gabrielli, H.C. Junqueira, D. B. Tada, D. Severino, R. de Fátima Turchiello, M.S. Baptista, Methylene blue in photodynamic therapy: from basic mechanisms to clinical applications, Photodiagnosis Photodyn. Ther. 2 (2005) 175–191, https://doi.org/10.1016/S1572-1000(05)00097-9.

[35] E.S. de Medeiros, C.A. França, C. da, C. Krewer, R. de, M. Peixoto, A.F. de Souza Júnior, M.B. Cavalcante, M.M. da Costa, R.A. Mota, Antimicrobial resistance of *Staphylococcus spp.* isolates from cases of mastitis in buffalo in Brazil, J. Vet. Diagn. Invest. 23 (2011) 793–796, https://doi.org/10.1177/1040638711407882.

[36] D. Aherne, D.M. Ledwith, M. Gara, J.M. Kelly, Optical Properties and Growth Aspects of Silver Nanoprisms Produced by a Highly Reproducible and Rapid Synthesis at Room Temperature, Adv. Funct. Mater. 18 (2008) 2005–2016, https://doi.org/10.1002/adfm.200800233.

[37] A.U. Khan, Y. Wei, Z.U. Haq Khan, K. Tahir, A. Ahmad, S.U. Khan, F.U. Khan, Q. U. Khan, Q. Yuan, Visible light-induced photodegradation of methylene blue and reduction of 4-nitrophenol to 4-aminophenol over bio-synthesized silver nanoparticles, Sep. Sci. Technol. 51 (2016) 1070–1078, https://doi.org/10.1080/01496395.2016.1140203.

[38] P.B. Johnson, R.W. Christy, Optical constants of the noble metals, Phys. Rev. B 6 (1972) 4370–4379, https://doi.org/10.1103/PhysRevB.6.4370.

[39] I. Kraljić, S. El Mohsni, A new method for the detection of SINGLET oxygen in AQUEOUS solutions, Photochem. Photobiol. 28 (1978) 577–581, https://doi.org/10.1111/j.1751-1097.1978.tb06972.x.

[40] T. Mosmann, Rapid colorimetric assay for cellular growth and survival: application to proliferation and cytotoxicity assays, J. Immunol. Methods 65 (1983) 55–63, https://doi.org/10.1016/0022-1759(83)90303-4.

[41] M.M. da Silva, T.A. Rocha, D.F. de Moura, C.A. Chagas, F.C.A. de Aguiar Júnior, N. P. da Silva Santos, R.V. Da Silva Sobral, J.M. do Nascimento, A.C. Lima Leite, L. Pastrana, R.M.P.B. Costa, T.P. Nascimento, A.L.F. Porto, Effect of acute exposure in swiss mice (Mus musculus) to a fibrinolytic protease produced by Mucor subtilissimus UCP 1262: an histomorphometric, genotoxic and cytological approach, Regul. Toxicol. Pharmacol. 103 (2019) 282–291, https://doi.org/10.1016/j.yrtph.2019.02.009.

[42] J.E. Millstone, S.J. Hurst, G.S. Métraux, J.I. Cutler, C.A. Mirkin, Colloidal Gold and Silver Triangular Nanoprisms, Small 5 (2009) 646–664, https://doi.org/10.1002/smll.200801480.

[43] P. Van Dong, C.H. Ha, L.T. Binh, J. Kasbohm, Chemical synthesis and antibacterial activity of novel-shaped silver nanoparticles, Int. Nano Lett. 2 (2012) 9, https://doi.org/10.1186/2228-5326-2-9.

[44] T. Theivasanthi, M. Alagar, Electrolytic synthesis and characterizations of silver nanopowder, Nano Biomed. Eng. 4 (2012) 58–65, https://doi.org/10.5101/nbe.v4i2.p58-65.

[45] J. Girard, P.S. Brunetto, O. Braissant, Z. Rajacic, N. Khanna, R. Landmann, A. U. Daniels, K.M. Fromm, Development of a polystyrene sulfonate/silver nanocomposite with self-healing properties for biomaterial applications, Comptes Rendus Chim. 16 (2013) 550–556, https://doi.org/10.1016/j.crci.2013.04.010.

[46] J. Andrade, C. González-Martínez, A. Chiralt, Effect of carvacrol in the properties of films based on poly (vinyl alcohol) with different molecular characteristics, Polym. Degrad. Stab. 179 (2020) 109282, https://doi.org/10.1016/j.polymdegradstab.2020.109282.

[47] S.P.C. Caplan, T.B.G. Silva, A.D.S. Franscisco, E.R. Lachter, R.S.V. Nascimento, Sulfonated polystyrene nanoparticles as oleic acid diethanolamide surfactant nanocarriers for enhanced oil recovery processes, Polym 11 (2019), https://doi.org/10.3390/polym11091513.

[48] I.M. Jipa, A. Stoica, M. Stroescu, L.-M. Dobre, T. Dobre, S. Jinga, C. Tardei, Potassium sorbate release from poly(vinyl alcohol)-bacterial cellulose films, Chem. Pap. 66 (2012) 138–143, https://doi.org/10.2478/s11696-011-0068-4.

[49] Y. Wang, Y. Shen, Y. Zhang, B. Yue, C. Wu, pH-Sensitive polyacrylic acid (PAA) hydrogels trapped with Polysodium-p-Styrenesulfonate (PSS), J. Macromol. Sci. Part B- Phys. 45 (2006) 563–571, https://doi.org/10.1080/00222340600770111.

[50] P.E. Cabral Filho, A.L.C. Cardoso, M.I.A. Pereira, A.P.M. Ramos, F. Hallwass, M.M. C.A. Castro, C.F.G.C. Geraldes, B.S. Santos, M.C. Pedroso de Lima, G.A.L. Pereira, A. Fontes, CdTe quantum dots as fluorescent probes to study transferrin receptors in glioblastoma cells, Biochim. Biophys. Acta - Gen. Subj. 1860 (2016) 28–35, https://doi.org/10.1016/j.bbagen.2015.09.021.

[51] S. Liao, Y. Zhang, X. Pan, F. Zhu, C. Jiang, Q. Liu, Z. Cheng, G. Dai, G. Wu, L. Wang, L. Chen, Antibacterial activity and mechanism of silver nanoparticles against multidrug-resistant Pseudomonas aeruginosa, Int. J. Nanomedicine 14 (2019) 1469–1487, https://doi.org/10.2147/IJN.S191340.

[52] M. Behravan, A. Hossein Panahi, A. Naghizadeh, M. Ziaee, R. Mahdavi, A. Mirzapour, Facile green synthesis of silver nanoparticles using Berberis vulgaris leaf and root aqueous extract and its antibacterial activity, Int. J. Biol. Macromol. 124 (2019) 148–154, https://doi.org/10.1016/j.ijbiomac.2018.11.101.

[53] A.U. Khan, Y. Wei, A. Ahmad, Z.U. Haq Khan, K. Tahir, S.U. Khan, N. Muhammad, F.U. Khan, Q. Yuan, Enzymatic browning reduction in white cabbage, potent antibacterial and antioxidant activities of biogenic silver nanoparticles, J. Mol. Liq. 215 (2016) 39–46, https://doi.org/10.1016/j.molliq.2015.12.019.

[54] T.M. Visarius, J.W. Stucki, B.H. Lauterburg, Stimulation of respiration by methylene blue in rat liver mitochondria, FEBS Lett. 412 (1997) 157–160, https://doi.org/10.1016/S0014-5793(97)00767-9.

[55] G. Lin, M. Lewandowska, Plasmon-enhanced fluorescence provided by silver nanoprisms for sensitive detection of sulfide, Sensors Actuators B Chem. 292 (2019) 241–246, https://doi.org/10.1016/j.snb.2019.04.054.

[56] L.J. Sherry, R. Jin, C.A. Mirkin, G.C. Schatz, R.P. Van Duyne, Localized surface plasmon resonance spectroscopy of single silver triangular nanoprisms, Nano Lett. 6 (2006) 2060–2065, https://doi.org/10.1021/nl061286u.

[57] M. Yamamoto, K. Shitomi, S. Miyata, H. Miyaji, H. Aota, H. Kawasaki, Bovine serum albumin-capped gold nanoclusters conjugating with methylene blue for efficient 1O2 generation via energy transfer, J. Colloid Interface Sci. 510 (2018) 221–227, https://doi.org/10.1016/j.jcis.2017.09.011.

[58] L. Misba, S. Kulshrestha, A.U. Khan, Antibiofilm action of a toluidine blue O-silver nanoparticle conjugate on Streptococcus mutans: a mechanism of type I photodynamic therapy, Biofouling 32 (2016) 313–328, https://doi.org/10.1080/08927014.2016.1141899.

[59] R. Bryaskova, D. Pencheva, S. Nikolov, T. Kantardjiev, Synthesis and comparative study on the antimicrobial activity of hybrid materials based on silver nanoparticles (AgNps) stabilized by polyvinylpyrrolidone (PVP), J. Chem. Biol. 4 (2011) 185, https://doi.org/10.1007/s12154-011-0063-9.

[60] C. Werner, A. Sobiraj, A. Sundrum, Efficacy of homeopathic and antibiotic treatment strategies in cases of mild and moderate bovine clinical mastitis, J. Dairy Res. 77 (2010) 460–467, https://doi.org/10.1017/S0022029910000543.

[61] A. Khan, T. Ahmed, M. Rizwan, N. Khan, Comparative therapeutic efficacy of Phyllanthus emblica (Amla) fruit extract and procaine penicillin in the treatment of subclinical mastitis in dairy buffaloes, Microb. Pathog. 115 (2018) 8–11, https://doi.org/10.1016/j.micpath.2017.12.038.

[62] F.P. Sellera, C.P. Sabino, M.S. Ribeiro, R.G. Gargano, N.R. Benites, P.A. Melville, F. C. Pogliani, In vitro photoinactivation of bovine mastitis related pathogens, Photodiagnosis Photodyn. Ther. 13 (2016) 276–281, https://doi.org/10.1016/j.pdpdt.2015.08.007.

[63] L.H. Moreira, J.C.P. de Souza, C.J. de Lima, M.A.C. Salgado, A.B. Fernandes, D.I. K. Andreani, A.B. Villaverde, R.A. Zângaro, Use of photodynamic therapy in the treatment of bovine subclinical mastitis, Photodiagnosis Photodyn. Ther. 21 (2018) 246–251, https://doi.org/10.1016/J.PDPDT.2017.12.009.

[64] D. He, A.M. Jones, S. Garg, A.N. Pham, T.D. Waite, Silver nanoparticle−Reactive oxygen species interactions: application of a charging−Discharging model, J. Phys. Chem. C. 115 (2011) 5461–5468, https://doi.org/10.1021/jp111275a.

[65] S.F.G. Vilela, J.C. Junqueira, J.O. Barbosa, M. Majewski, E. Munin, A.O.C. Jorge, Photodynamic inactivation of Staphylococcus aureus and Escherichia coli biofilms by malachite green and phenothiazine dyes: an in vitro study, Arch. Oral Biol. 57 (2012) 704–710, https://doi.org/10.1016/j.archoralbio.2011.12.002.

[66] L.H. Alvarenga, R.A. Prates, T.M. Yoshimura, I.T. Kato, L.C. Suzuki, M.S. Ribeiro, L. R. Ferreira, S.Ados S. Pereira, E.F. Martinez, E. Saba-Chujfi, Aggregatibacter actinomycetemcomitans biofilm can be inactivated by methylene blue-mediated photodynamic therapy, Photodiagnosis Photodyn. Ther. 12 (2015) 131–135, https://doi.org/10.1016/J.PDPDT.2014.10.002.

[67] V. Pérez-Laguna, A. Rezusta, J.J. Ramos, L.M. Ferrer, J. Gené, M.J. Revillo, Y. Gilaberte, Daylight photodynamic therapy using methylene blue to treat sheep with dermatophytosis caused by Arthroderma vanbreuseghemii, Small Rumin. Res. 150 (2017) 97–101, https://doi.org/10.1016/j.smallrumres.2017.03.011.

[68] P. Abreu Villela, N. de, C. de Souza, J.D. Baia, M.A. Gioso, A.C.C. Aranha, P.M. de Freitas, Antimicrobial photodynamic therapy (aPDT) and photobiomodulation (PBM – 660nm) in a dog with chronic gingivostomatitis, Photodiagnosis Photodyn. Ther. 20 (2017) 273–275, https://doi.org/10.1016/j.pdpdt.2017.10.012.

[69] A. Azizi, P. Shohrati, M. Goudarzi, S. Lawaf, A. Rahimi, Comparison of the effect of photodynamic therapy with curcumin and methylene Blue on streptococcus mutans bacterial colonies, Photodiagnosis Photodyn. Ther. 27 (2019) 203–209, https://doi.org/10.1016/J.PDPDT.2019.06.002.

[70] F. Daliri, A. Azizi, M. Goudarzi, S. Lawaf, A. Rahimi, In vitro comparison of the effect of photodynamic therapy with curcumin and methylene blue on Candida albicans colonies, Photodiagnosis Photodyn. Ther. 26 (2019) 193–198, https://doi.org/10.1016/j.pdpdt.2019.03.017.

[71] Z. Malá, L. Žárská, R. Bajgar, K. Bogdanová, M. Kolář, A. Paláček, S. Binder, H. Kolářová, The application of antimicrobial photodynamic inactivation on methicillin-resistant S. Aureus and ESBL-producing K. Pneumoniae using porphyrin photosensitizer in combination with silver nanoparticles, Photodiagnosis Photodyn. Ther. 33 (2021) 102140, https://doi.org/10.1016/j.pdpdt.2020.102140.

APÊNDICE B - ARTIGO 2 – SILVER NANOPRISMS@METHYLENE BLUE CONJUGATES AS A STRATEGY IN PHOTODYNAMIC INACTIVATION AGAINST CANDIDA ALBICANS ISOLATED FROM BALANITIS IN VITRO

A ser submetido a Photodiagnosis and Photodynamic Therapy
Fator de impacto: 3.631 (2020) – Qualis de área (Farmácia): A2

Silver nanoprisms@methylene blue conjugates as a strategy against *Candida albicans* isolated from balanoposthitis in vitro using photodynamic inactivation

Introduction

Balanoposthitis is defined as an inflammation of the glans penis in uncircumcised men. It can occur due to different factors, such as hygiene, infections, skin disorders and also due to decreased immunity due to other diseases, such as diabetes mellitus [1]. Balanoposthitis can manifest itself in different ways. Among them, we have the inflammatory, which is characterized by the presence of lichens, and the neoplastic, which is related to malignant lesions, such as in Bowen's disease and in allergies, such as to latex and chlorine when associated with lack of hygiene [2]. Another cause is infection, which can be caused by microorganisms, and corresponds to the large number of cases observed where the disease is recurrent [2]. The main microorganism associated with this condition is *Candida albicans*, a commensal species, responsible for about 30 to 35% of infections [1,3]. Some other fungi, such as *Aspergillus spp*. and dermatophytes are also frequently isolated, as well as some bacteria, such as *Staphylococcus spp.* and Group B and D *Streptococcus* [3]. Although some patients may be asymptomatic, some itching may be found, as well as changes in the glans, involving fissures [3,4].

Between alternative methods currently studied for fungus inactivation, Photodynamic Therapy (PDT) is a non-invasive technique that uses a light source in resonance with a sensitive molecule (known as a photosensitizer, PS) and molecular oxygen [5]. Through several reactions, the so-called reactive oxygen species (ROS) will be generated, which have cytotoxic action, and kill the target at the site of action [6]. It is a technique that has already shown good results for strains of bacteria, fungi, parasites and also cancer cells. Several molecules are used as PS, among them we have methylene blue. It is widely used because of its low cost and good efficiency in generating EROS. There are already reports of its use in the field of dentistry, in the killing of bacteria, fungi and also combined with nanomaterials to improve its photodynamic efficiency. In the fungal field, PDT was related to photodynamic inactivation of several species, such as *Candida*, with several PS and various parameters [7,8] and reports of prevention of aggregation in biofilms [9,10].

Nanotechnology can be an important tool for enhancement of PS efficacy, and the association of PS to metallic nanoparticles has shown advantages such as high stability, adjustable size, unique optical properties, and easy surface functionalization, making them very biocompatible. Most applied systems are gold nanoparticles (AuNPs) and silver nanoparticles (AgNPs) [11].One of the mechanisms proposed to enhance PS efficacy are related to Localized Surface Plasmon Resonance (LSPR) of NPs, that corresponds to collective oscillation of

electrons present at the surface of the particles [12]. This phenomenon is dependent on NPs size and shape and for some conditions, such as spectral distance, these electrons can be transferred to fluorophore molecules and then enhance their action [13].

In our previous work [14], we showed photodynamic inactivation of *Staphylococcus aureus* isolated from bubaline mastitis, a strain multi resistant to 19 antibiotics associations. A conjugate involving MB at final concentration of 45 μmol.L^{-1} and nanoprisms was produced and characterized, and we were able to reduce photodynamic inactivation time from 9 to 6 minutes compared to MB solution with the same concentration. Herein, we aim to deepen the discussion about efficacy of these conjugates, improving MB dosage and overseeing silver nanoparticles influence of the NPs in order to understand the nature of the observed effect, whether it is linked to the presence of the nanoparticles themselves, or else, are plasmon related.

Materials and Methods

2.1 Materials

Silver nitrate (>99%), trisodium citrate dibasic (>99%), L-Ascorbic acid (>99%), poly (sodium 4-styrenesulfonate, 1.000 kDa), sodium borohydride (>98%), sabouraud 4% dextrose agar, potassium phosphate monobasic (99%) and potassium phosphate dibasic (99%) were purchased from Sigma Aldrich. Methylene blue (99%) was purchased from Merck.

2.2 Synthesis of silver nanoprisms using seed-mediated growth method

Nanoprisms were synthesized adapting the previously described methodology [15]. Basically, in an Erlenmeyer flask at RT (~26ºC) and under vigorous stirring (~750 rpm), 5 mL of TSC (2.5 mmol.L^{-1}), 1.250 mL of PSSS (500 mg.mL^{-1}), 1 .5 mL of $NaBH_4$ (10 mmol.L^{-1}) and 10 mL of $AgNO_3$ (0.5 mmol.L^{-1}) were thoroughly mixed. The system was stirred for 3 min after the addition of all the Ag^+ solution, and then, it was set aside. For the growth of the nanoprisms, we applied 50 mL of deionized water under the same conditions of the seed production system. To this system, 750 μL of $C_6H_8O_6$ (ascorbic acid, 10 mmol.L^{-1}) and 2 mL of the prepared seed suspension were added. 15 mL of $AgNO_3$ (0.5 mmol.L^{-1}) was added drop wise, observing the color change to dark blue. Finally, 5 mL of TSC (25 mmol.L^{-1}) was added. Systems were characterized by absorption spectroscopy in the UV-vis region, from 350 to 900 nm.

2.3 MBNP association

First, nanoprism systems were purified using filtration tubes with a molecular cut-off of 10 kDa (General Electrics) removing interferences and impurities. Particles were redispersed to the same initial volume. Then, the conjugates were produced by electrostatic association of MB, through the addition of equal volumes of both systems resulting conjugates named herein MBNP. MB solution was added to the systems, in order to a final concentration of 25 µmol.L^{-1} (MBNP1), 50 µmol.L^{-1} (MBNP2) and 100 µmol.L^{-1} (MBNP3). The systems were kept under agitation (~750 rpm) for 24h in the absence of light, at 25ºC prior to the experiments.

2.4 Characterization

All systems were characterized using absorption and emission electron spectroscopy. All acquiring spectral conditions were kept the same for all the samples. For nanoprisms and conjugates, the measurement of the zeta potential (Malvern, UK) was performed by diluting 5 mL the conjugate suspensions in 50 mL of deionized water (pH = 6.9). Transmission electronic images were acquired using a FEI Tecnai Spirit Biotwin G2 (120 V) and the samples were prepared by dropping *ca*. 10 µL of the purified suspension and letting them dry prior to the image acquisition. Images were analyzed by *ImageJ* software program and several images were screened for statistical purposes.

2.5 Inoculum nutrition and standardization

Inoculum used for the study was provided by the Coleção de Cultura de Microrganismos Profª Maria Nelly Pisciottano, from Laboratório de Análises Microbiológicas/UFPE. Strain used in this study was isolated from balanoposthitis and showed resistance to fluconazole. For activation, one layer was subcultured on sabouraud dextrose agar, and incubated for 24 h at 37ºC in a bacteriological oven. For the preparation of the suspension, the absorbance was standardized in 0.284 at 530 nm (corresponding to 10^6 CFU/mL).

2.6 Photodynamic inactivation

For inactivation, the methodology was based on that proposed by Rodrigues et al, (2021) [14]. As a light source, the LEDBox λ = 660 nm was used, coupled with Smart Control and Dark Chamber, with an irradiance of 45.87 mW/cm^2. A pre-incubation time (PIT) of 30 minutes was applied. Using a 96-well plate, 100 µL of the isolate suspension was added with the subsequent addition of 100 µL of the tested conjugate suspension. After the incubation, each plate was exposed to irradiation times of 60, 120, 180 and 240s *(i.e.* radiant exposures of 2.08, 5.06, 8.03 and 11 J.cm^{-2}).

Subsequently, each test was serially diluted from 10^{-1} to 10^{-4}, and 10 µL was dropped vertically onto a plate with sabouraud dextrose agar. The plates were incubated in a bacteriological oven at 37ºC for 24h, and the smallest dilution with observed fungal growth was counted and converted to Log_{10}. A control following all the conditions described above, was performed only with the AgNPr, to verify if the same effect was observed from these systems.

Results

3.1 Silver nanoprisms structural characterization

Transmission electron microscopy images showed an average size of d = 37 ± 9 nm in close agreement to a previous report [14]. Figure 1 shows a representative image of the AgNPr applied in the present study. The histogram (Fig. 1b) shows the analysis of several TEM images.

Figure 1 - TEM images for AgNPr particles showing nanoplatelets morphology (a) and size distribution of AgNPr (b).

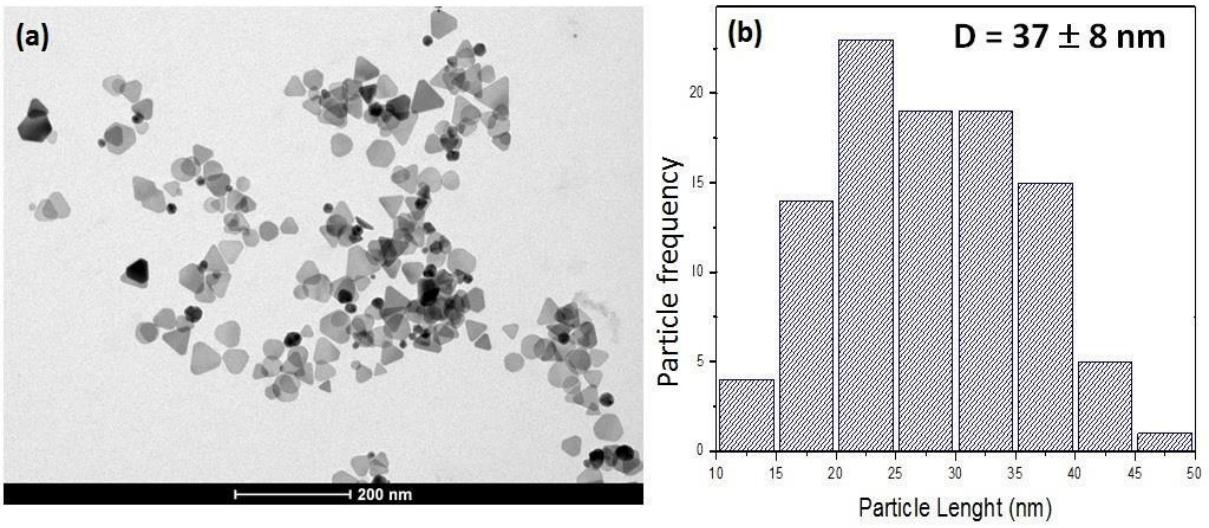

Although some spheric seeds and hexagonal shaped particles are still observed among the prismatic platelets they represent less than 10% of the whole ensemble.

Zeta potential measurement of AgNPr particles showed as expected, a very negative value (ζ = -51.4 mV) indicating a great stability of the colloidal system, and that PSSS chains are coating the particles. The conjugation of the MB cationic species to PSSS coated silver nanoprisms was monitored by determining the zeta potential change with the increase in MB concentration and data are shown in Figure 2. This shows that indeed the MB is associating to the sulfate terminations of the PSSS polymer chain.

Figure 2 - Zeta potential of AgNPr and MBNP conjugates prepared in this study. Data are disposed as mean ± SDand correspond to 3 different measures (n = 3).

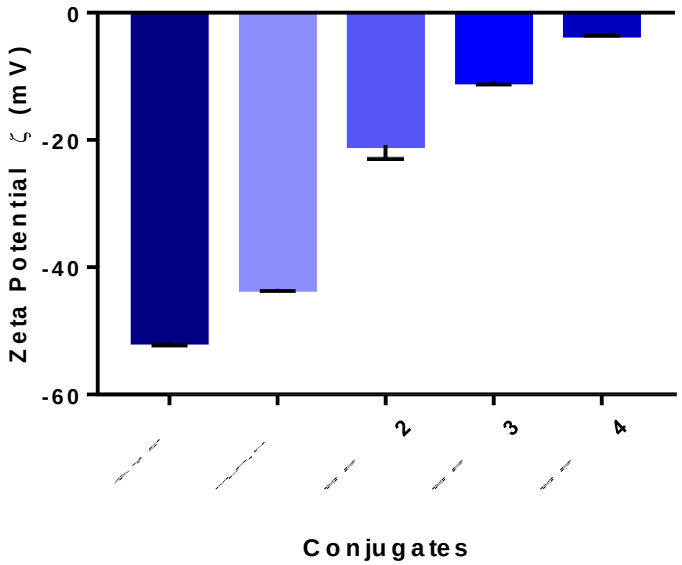

Based on the description of the surface charge we suggest that the MB coating of the particles may be represented as the scheme in Figure 3.

Figure 3 - Schematic representation of MBNP conjugates prepared in the present study. AgNPr representthe prismatic nanoplatelets coated with anionic PSSS polymer.

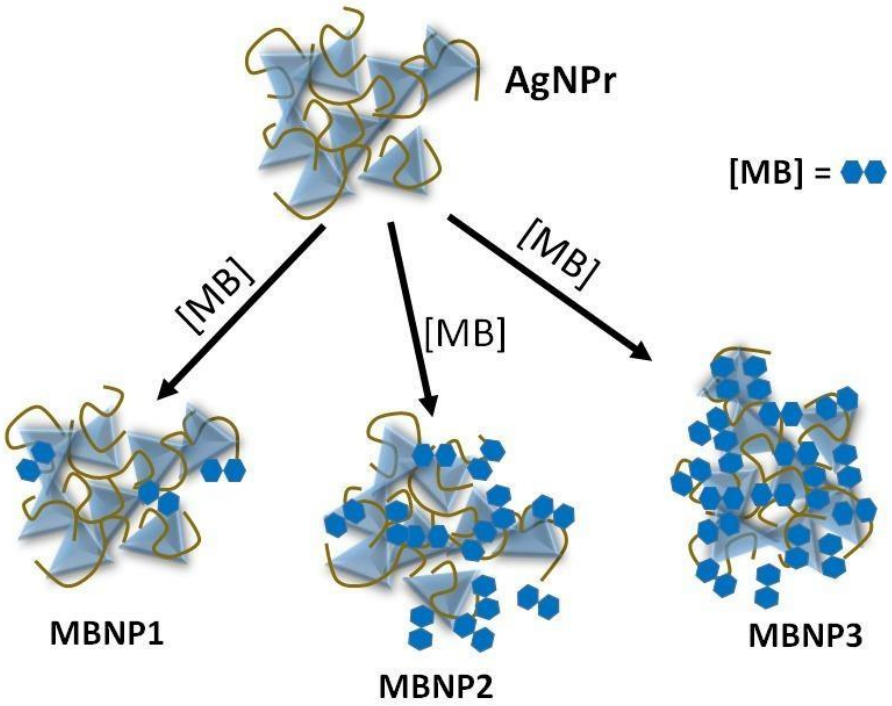

As the surface charge is approximating the neutrality in the MBNP4 conjugates, we suggest that the sulfate sites are almost completely associated to MB species. No macroscopic alterations (color change or precipitation) of the conjugated systems were observed, and the systems remained stable for at least three months.

3.2 Optical characterization of the systems

In the first step of synthesis, we achieved spherical nanoparticles stabilized by PSSS polymer chains, that present extinction band with maximum at λ = 408 nm (Figure 4, orange line). Using 2 mL of this seed suspension, we induced the growth of nanoprisms with a maximum peak at λ = 664 nm (Fig 4, blue line) and this spectral shift agrees with the formation of silver prismatic nanoplatelets (AgNPr) already reported in the literature [12,13]. In Figure 4(b) we observe methylene blue characteristic absorption spectrum. We may observe a total spectral overlap of the MB and the AgNPr absorption bands.

Figure 4 - Extinction spectra of spherical silver nanoparticles (known as seeds) with maximum at 408 nm and silver nanoprisms (AgNPr) with a maximum at 664 nm (a) and normalized absorption spectra of AgNPr and MB solution (b).

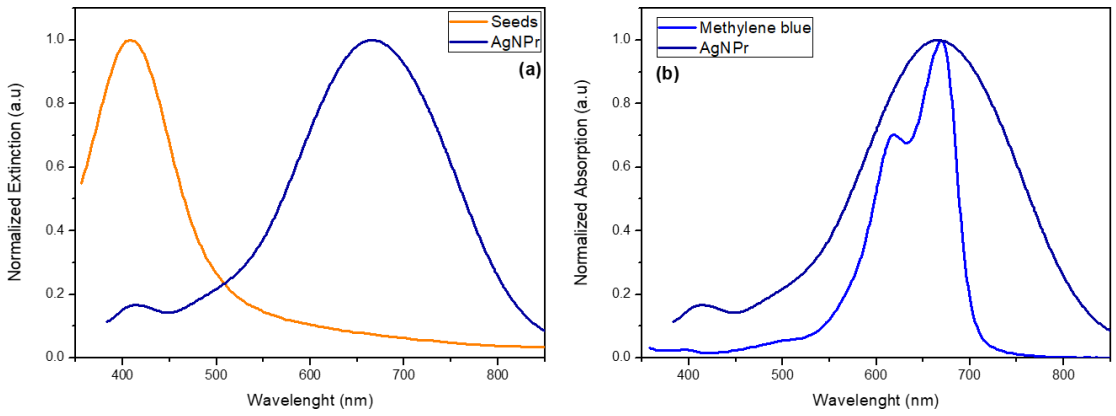

Fig 5(a) shows the absorption spectra of three different concentrations of MB solution (25, 50 and 100 μmol.L^{-1}). It is composed of two bands, the more blue shifted band represents the dimerized MB species, always present. At the greatest concentration this component increases substantially, evidencing a higher amount of dimerized molecules. This is a known effect [16] and it is usually related to the decrease in photodynamic ation of this PS. Absorption spectra of MBNP conjugates with increasing MB concentration are depicted in Fig 5(b) and we observe a very close resemblance to the MB corresponding solution spectrum. Nevertheless,

the small increase in the baseline and wider shape of the band profile, specially for the smaller MB concentration associated to the silver particles, show the influence of the silver nanoparticles absorption profile. This contribution completely disappears for the greater MB concentration and moreover, the dimerization effect is highly decreased.

While silver nanoprisms do not show detectable fluorescence, MB species show red emission in the solutions, as well as, associated to the silver nanoparticles. There are two features that are worth mentioning: (i) linear decrease in the fluorescence emission intensity for the MB species in solution, with increasing concentration and (ii) the conjugated systems show the characteristic emission profile of MB, but present an increase of the emission intensity with MB concentration increment. This contrasting behavior is depicted in Figure 6, which shows the variation of the emission intensity for both systems.

Figure 5 - Absorption spectra of (a) Methylene blue solutions and (b) MBNP conjugates. Emission profiles of methylene blue solutions (c) and MBNP conjugates (λex = 660 nm).

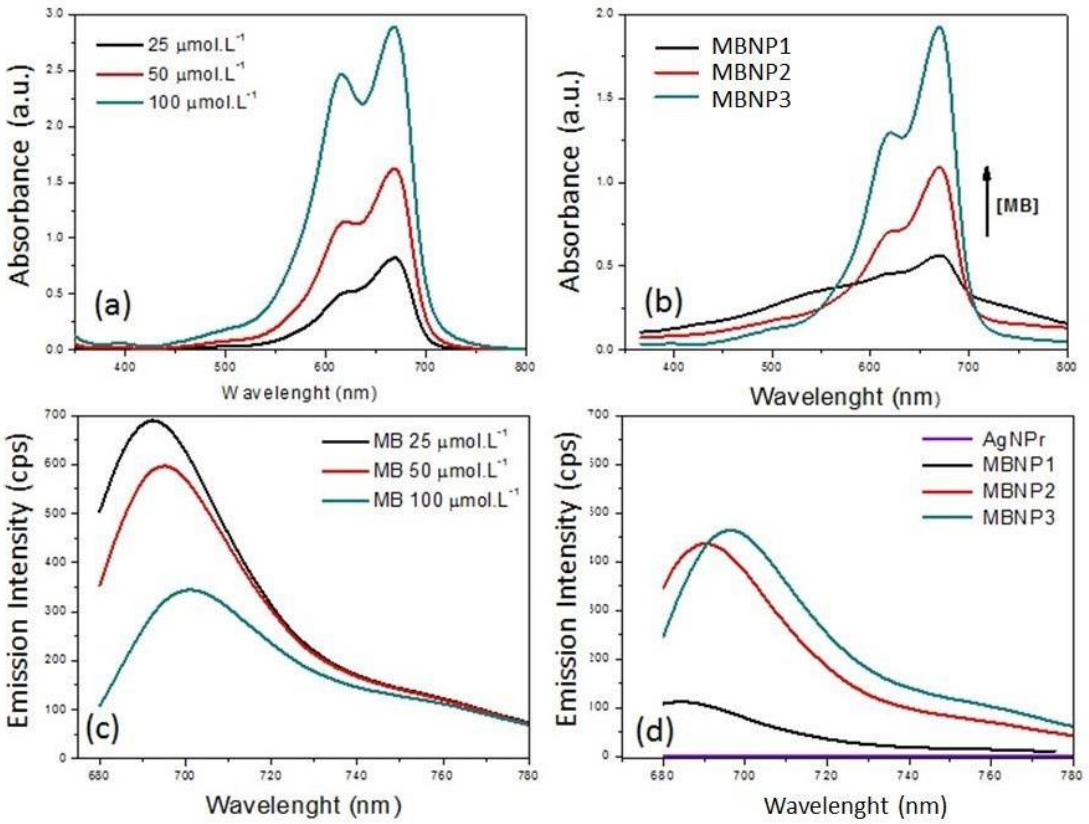

Figure 6 - Emission intensity variation of MB (red) and MBNP (blue) with increasing MB concentration.

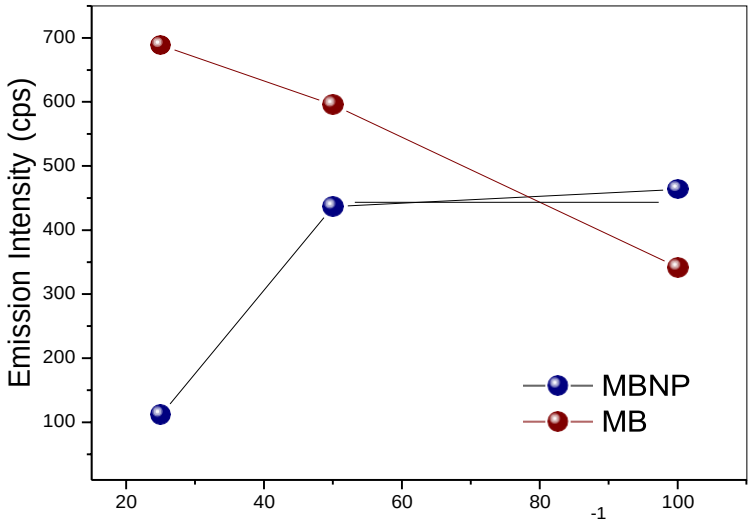

[MB concentration] μmol.L

Interestingly, emission of methylene blue associated to AgNPr particles presented an increase in intensity according to the increase in MB associated at their surface. For the highest MB concentration (100 μmol.L^{-1}) we observed na increase of ca. 35% of the emission intensity.

3.3 In vitro photodynamic inactivation

The irradiation of red light without any photosensitizer or only applying MB or MBNP without light irradiation were not able to kill fungal strains at any scenario tested in the present study. As a positive control, chlorhexidine 0.12% killed the strains in all experiments. For inactivation with MB, we observed some effect (~ 1 log) only with the higher irradiation time. For the conjugate at the lowest MB concentration, no significant effect was observed, reducing only less than a log. None of the conjugates promoted cell death in the absence of light, showing that the conjugates alone are not responsible for this effect to be achieved. Increasing the dose of methylene blue in the conjugates, it was possible to observe that we had an improvement in the photodynamic effect. Total inactivation was achieved with different minutes according to MB concentrations on conjugates. Figure 7 presents all the results.

Figure 7 - Photodynamic inactivation of *C. albicans* isolated from balanoposthitis using MB in solution and MBNP conjugates, under irradiation of red light (45.87 mW.cm^{-2} of irradiance) and irradiance times of 60, 120, 180 and 240 s (radiant exposure of 2.08, 5.06, 8.03 and 11 J.cm^{-2}). Results are disposed as mean ± SD of three independent experiments (n = 3) * $p < 0.05$ vs. Control group.

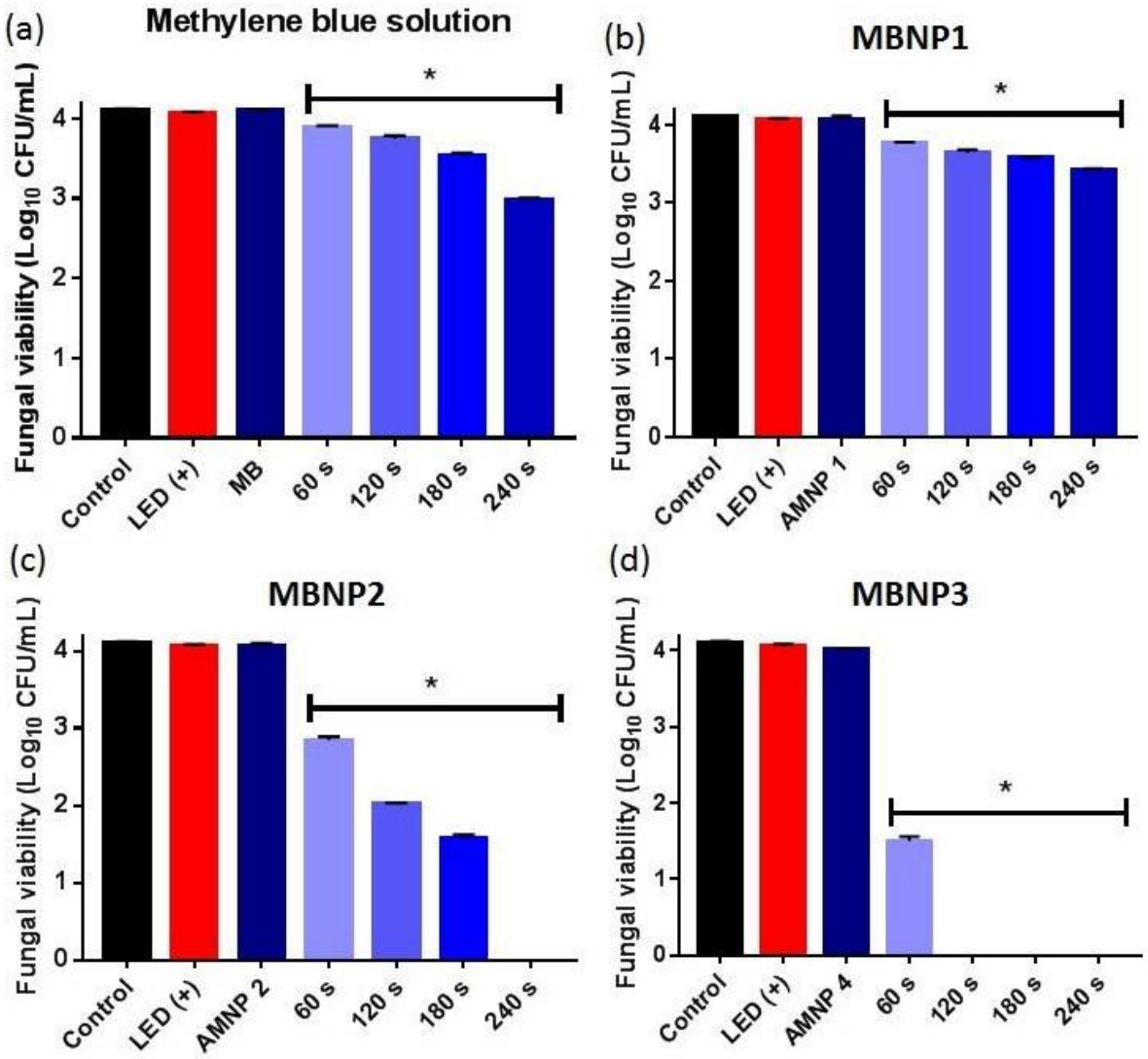

Discussion

Nanoparticles are constantly studied to improve the properties of FS, with the greater amount of studies related to gold nanoparticles [17,18] or spherical silver particles [19–21]. In our previous work, a very efficient inactivation of *Staphylococcus aureus* isolated from buffalo mastitis was shown, using the association of MB and silver nanoprisms that presented full spectral overlap to MB species [14]. The main objective in the present study, fully correlated to the previous one, was to probe the concentration effect in the association of methylene blue with silver nanoprisms with similar optical properties, analyzing the concentration variation on the photodynamic action of MB in the conjugate, keeping constant same amount of NPs.

Transmission electron microscopy analysis of the silver nanoparticles showed an ensemble of prismatic platelets, with an average size of 37 ± 8 nm with residual seeds and

hexagonal particles (less than 10%). The electrostatic conjugation was successfully monitored by zeta potential changes at the surface of the negative PSSS coated AgNPrs.

Analyzing the spectral changes observed with increasing MB species attached to the nanoparticles (Fig. 5) we suggest that, as observed in the zeta potential behavior of the conjugates (Fig. 3), the lower the concentration of MB species, the greater the optical interference of the AgNPrs. Although a small amount silver nanoparticles is used in the systems, their absorption band is still perceptible in the overlapped graphs. In MBNP2 we still observe the result of overlapping both absorption bands. However, this effect finally disappears in MBNP3 conjugates. In this latter system, MB contribution is dominant in the spectra (Fig. 5b). Moreover, in Figure 5(c) we observe that the emission intensity of MB decreased with increasing concentration of this species and this effect is probably related to the characteristic self-quenching of the fluorescence due to excess competing species [22]. This effect was not observed in the MB conjugates. The emission intensity variation of both systems is described in Figure 6. While MB solutions present self-quenching of the emission for increasing [MB], for the MBNP conjugates we observe an increase of the fluorescence intensity with the [MB] reaching the highest intensity at 100 $mmol.L^{-1}$. Indeed, we observed that MBNP3 presented an increase of *ca.* 35.08% in intensity when compared to MB at a concentration of 100 $\mu mol.L^{-1}$. We strongly believe that this behavior may be related to the association of MB species to the Ag nanoparticles. This association promotes several effects that may explain the optical behavior observed: (i) MB dimerization process is decreased by sequestering them by sulfate groups of the PSSS polymer chains; (ii) as the particles are not free in solution and are probably kept in a greater distance from each other, the self-quenching induced by increase of MB concentration is prevented (iii) fully coating of the AgNPrs by the MB species decreases their competition of the excitation light used in the experiment rendering a more efficient excitation of the MB species and (iv) the proximity of MB species to the metallic surface may promote a greater emission output by surface plasmonic effect. As shown in our previous study, the Ag nanoprisms prepared, and that were also applied in the present study, present *ca.* 30% electric field enhancement at their surface, calculated to be at the terminations of the prismatic nanoplatelets [14]. This allows for a greater plasmonic enhancement.

According to Ribeiro et al (2018) [23], loading of PS onto NPs can influence the energy transfer process. In addition to the distance between the molecules, charge can help or decrease the effect, and also the presence of other biomolecules can contribute to the increase of the effect. Pectin proved that its presence on the surface of spherical nanoparticles allowed the activation of FS to occur, so that the desired effect was obtained [23].

Different strategies have already been used to improve the parameters of photodynamic therapy using methylene blue. Among them, we have their incorporation in latex membranes to inactivate *C. albicans* [24], combined with AuNPs or spherical AgNPs for the treatment of MDA-MB-468 cell lineage (breast cancer) [20], combined with spherical AgNPs for bacterial photodynamic inactivation [25], among other similar reports. In all these studies, the dose of MB used is much higher than what we applied in this work. We strongly believe that the effect observed at lower MB concentrations is due to the optical overlap between MB and AgNPr as well as their proximity induced by electrostatic association, inducing plasmonic enhancement. According to Belekov et al (2020) [25], a germicidal effect may come from the association between AgNPs and MB, when these are spherical, due to the smaller size of these particles, which allow entry into microorganisms and act via the antibacterial mechanism of silver. Due to their size (30-40 nm), entry into microorganisms is difficult, which suggests that the prisms are in fact anchoring on the fungal surface and (i) either bonding with sulfur-containing proteins or (ii) being attracted to the negative ell wall by the MB species, promoting the effect on the cell wall [26,27]. It is worth mentioning that applying only AgNPr systems to *C. albicans* isolates with and without light radiation did not show photodynamic action, preserving cell viability.

When using only MB for the photosensitizing action, compared to the highest dose of the conjugate, we observed that the inactivation, although still not attractive, was dose dependent. Studies with *Candida albicans* show that high doses of MB (*i.e.* doses higher than 20 $mg.L^{-1}$) can cause PS aggregation and reduce the photodynamic efficacy. Using a 100 $\mu mol.L^{-1}$, Oliveira-Silva et al, (2019) [28] observed inactivation of *Candida albicans* isolates, but this effect was obtained applying a 4 times higher radiant exposure than compared to our experiment. Nevertheless, we increased the efficiency of MB action by associating them to the silver nanoprisms. Using MBNP3, we decreased irradiation time to 2 min for full inactivation of this isolate, and MBNP2 (50 $\mu mol.L^{-1}$) inactivated the same strain within 4 min. Negligible inactivation was observed for MBNP1 and we believe that this results from a smaller number of MB molecules *per* particle. As far as we observed, there is no report of using silver nanoprisms with MB to inactivate *Candida* species and we believe that silver nanoprisms may be applied as news plasmonic tunable tool to enhance a great number of photosensitizers aiming at photoinduced cell inactivation.

Conclusion

In this work, MB association with silver nanoprisms (30-40 nm) showed that we can successfully inactivate *Candida albicans* isolated from balanoposthitis with reduced irradiation time. MBNP systems showed higher stability and no toxicity, being suggested as a new tool for enhancing photodynamic applications with size tuning capability.

Acknowledgements

The authors are grateful to Conselho Nacional Científico e Tecnológico (CNPq, Grant Nr 424235/2018-8), Coordenação de Aperfeiçoamento de Pessoal de Nível Superior (Capes, for scholarship of C. H. Rodrigues) and Fundação de Amparo à Ciência e Tecnologia do Estado de Pernambuco (FACEPE, APQ-0573-2.09/18 and BIC 1431-4.03/21). This work is linked to National Institute of Photonics (INCT-INFo).

References

[1] C. Lisboa, A. Santos, C. Dias, F. Azevedo, C. Pina-Vaz, A. Rodrigues, Candida balanitis: risk factors, J. Eur. Acad. Dermatology Venereol. 24 (2010) 820–826. https://doi.org/https://doi.org/10.1111/j.1468-3083.2009.03533.x.

[2] O.S. Perkins, S. Cortes, Balanoposthitis., in: Treasure Island (FL), 2022.

[3] Y. Hu, Y. Hu, Y. Lu, S. Huang, K. Liu, X. Han, Z. Mao, Z. Wu, X. Zhou, A Case Report of Penile Infection Caused by Fluconazole- and Terbinafine-Resistant Candida albicans., Mycopathologia. 182 (2017) 397–402. https://doi.org/10.1007/s11046-016-0070-z.

[4] I. Maatouk, M.A. Hajjar, R. Moutran, Candida albicans and Streptococcus pyogenes balanitis: diabetes or STI?, Int. J. STD AIDS. 26 (2015) 755–756. https://doi.org/10.1177/0956462414555933.

[5] S. Kwiatkowski, B. Knap, D. Przystupski, J. Saczko, E. Kędzierska, K. Knap-Czop, J. Kotlińska, O. Michel, K. Kotowski, J. Kulbacka, Photodynamic therapy – mechanisms, photosensitizers and combinations, Biomed. Pharmacother. 106 (2018) 1098–1107. https://doi.org/https://doi.org/10.1016/j.biopha.2018.07.049.

[6] A.L.P. Silvestre, L.D. Di Filippo, J.F. Besegato, S.R. de Annunzio, B. Almeida Furquim de Camargo, P.B.G. de Melo, A.N. de S. Rastelli, C.R. Fontana, M. Chorilli, Current applications of drug delivery nanosystems associated with antimicrobial photodynamic therapy for oral infections, Int. J. Pharm. 592 (2021) 120078. https://doi.org/https://doi.org/10.1016/j.ijpharm.2020.120078.

[7] F. Alves, J.C. Carmello, E.G. de O. Mima, C.A. de S. Costa, V.S. Bagnato, A.C. Pavarina, Photodithazine-mediated antimicrobial photodynamic therapy against fluconazole-resistant Candida albicans in vivo, Med. Mycol. 57 (2019) 609–617. https://doi.org/10.1093/mmy/myy083.

[8] F. Daliri, A. Azizi, M. Goudarzi, S. Lawaf, A. Rahimi, In vitro comparison of the effect of photodynamic therapy with curcumin and methylene blue on Candida albicans colonies, Photodiagnosis Photodyn. Ther. 26 (2019) 193–198. https://doi.org/https://doi.org/10.1016/j.pdpdt.2019.03.017.

[9] J.C. Carmello, F. Alves, F.G. Basso, C.A. de Souza Costa, A.C. Tedesco, F. Lucas Primo, E.G. de O. Mima, A.C. Pavarina, Antimicrobial photodynamic therapy reduces adhesion capacity and biofilm formation of Candida albicans from induced oral candidiasis in mice, Photodiagnosis Photodyn. Ther. 27 (2019) 402–407. https://doi.org/https://doi.org/10.1016/j.pdpdt.2019.06.010.

[10] J. Ma, H. Shi, H. Sun, J. Li, Y. Bai, Antifungal effect of photodynamic therapy mediated by curcumin on Candida albicans biofilms in vitro, Photodiagnosis Photodyn. Ther. 27 (2019) 280–287. https://doi.org/https://doi.org/10.1016/j.pdpdt.2019.06.015.

[11] L. Shang, X. Zhou, J. Zhang, Y. Shi, L. Zhong, Metal Nanoparticles for Photodynamic Therapy: A Potential Treatment for Breast Cancer, Mol. . 26 (2021). https://doi.org/10.3390/molecules26216532.

[12] J.E. Millstone, S.J. Hurst, G.S. Métraux, J.I. Cutler, C.A. Mirkin, Colloidal Gold and Silver Triangular Nanoprisms, Small. 5 (2009) 646–664. https://doi.org/10.1002/smll.200801480.

[13] M. Li, S.K. Cushing, N. Wu, Plasmon-enhanced optical sensors: a review, Analyst. 140 (2015) 386–406. https://doi.org/10.1039/C4AN01079E.

[14] C.H. Rodrigues, E.A.G. Araújo, R.P. Almeida, T.P. Nascimento, M.M. Silva, G. Abbas, F.D. Nunes, E. Lins, M.C.B. Lira-Nogueira, J.S.A. Falcão, A. Fontes, A.L.F. Porto, G. Pereira, B.S. Santos, Silver nanoprisms as plasmonic enhancers applied in the photodynamic inactivation of Staphylococcus aureus isolated from bubaline mastitis, Photodiagnosis Photodyn. Ther. 34 (2021) 102315. https://doi.org/https://doi.org/10.1016/j.pdpdt.2021.102315.

[15] D. Aherne, D.M. Ledwith, M. Gara, J.M. Kelly, Optical Properties and Growth Aspects of Silver Nanoprisms Produced by a Highly Reproducible and Rapid Synthesis at Room Temperature, Adv. Funct. Mater. 18 (2008) 2005–2016. https://doi.org/10.1002/adfm.200800233.

[16] J.P. Tardivo, A. Del Giglio, C.S. de Oliveira, D.S. Gabrielli, H.C. Junqueira, D.B. Tada, D. Severino, R. de Fátima Turchiello, M.S. Baptista, Methylene blue in photodynamic therapy: From basic mechanisms to clinical applications, Photodiagnosis Photodyn. Ther. 2 (2005) 175–191. https://doi.org/https://doi.org/10.1016/S1572-1000(05)00097-9.

[17] P. García Calavia, G. Bruce, L. Pérez-García, D.A. Russell, Photosensitiser-gold nanoparticle conjugates for photodynamic therapy of cancer, Photochem. Photobiol. Sci. 17 (2018) 1534–1552. https://doi.org/10.1039/C8PP00271A.

[18] I. Maliszewska, E. Wanarska, A.C. Thompson, I.D.W. Samuel, K. Matczyszyn, Biogenic Gold Nanoparticles Decrease Methylene Blue Photobleaching and Enhance Antimicrobial Photodynamic Therapy, Mol. . 26 (2021). https://doi.org/10.3390/molecules26030623.

[19] M.B. Rivas Aiello, D. Castrogiovanni, J. Parisi, J.C. Azcárate, F.S. García Einschlag, T. Gensch, G.N. Bosio, D.O. Mártire, Photodynamic Therapy in HeLa Cells Incubated with Riboflavin and Pectin-coated Silver Nanoparticles, Photochem. Photobiol. 94 (2018) 1159–1166. https://doi.org/https://doi.org/10.1111/php.12974.

[20] V.P.S. Jesus, L. Raniero, G.M. Lemes, T.T. Bhattacharjee, P.C. Caetano Júnior, M.L. Castilho, Nanoparticles of methylene blue enhance photodynamic therapy, Photodiagnosis Photodyn. Ther. 23 (2018) 212–217. https://doi.org/https://doi.org/10.1016/j.pdpdt.2018.06.011.

[21] P.G. Mahajan, N.C. Dige, B.D. Vanjare, S.-H. Eo, S.-Y. Seo, S.J. Kim, S.-K. Hong, C.-S. Choi, K.H. Lee, A potential mediator for photodynamic therapy based on silver nanoparticles functionalized with porphyrin, J. Photochem. Photobiol. A Chem. 377 (2019) 26–35. https://doi.org/https://doi.org/10.1016/j.jphotochem.2019.03.034.

[22] W. Bae, T.-Y. Yoon, C. Jeong, Direct evaluation of self-quenching behavior of fluorophores at high concentrations using an evanescent field, PLoS One. 16 (2021) e0247326. https://doi.org/10.1371/journal.pone.0247326.

[23] M.S. Ribeiro, L.S.A. de Melo, S. Farooq, A. Baptista, I.T. Kato, S.C. Núñez, R.E. de Araujo, Photodynamic inactivation assisted by localized surface plasmon resonance of silver nanoparticles: In vitro evaluation on Escherichia coli and Streptococcus mutans, Photodiagnosis Photodyn. Ther. 22 (2018) 191–196. https://doi.org/https://doi.org/10.1016/j.pdpdt.2018.04.007.

[24] M.A. O. Sousa, M.A.C. de Faria, R.P. Ribeiro, J.V.P. Valverde, H.D. Rocha, K.F. dos Santos, M.S. Sousa, P.C.S. Souto, J.R. Silva, N.C. de Souza, Latex membranes with

methylene blue dye for antimicrobial photodynamic therapy, Photochem. Photobiol. Sci. 20 (2021) 1027–1032. https://doi.org/10.1007/s43630-021-00077-z.

[25] E. Belekov, K. Kholikov, L. Cooper, S. Banga, A.O. Er, Improved antimicrobial properties of methylene blue attached to silver nanoparticles, Photodiagnosis Photodyn. Ther. 32 (2020) 102012. https://doi.org/https://doi.org/10.1016/j.pdpdt.2020.102012.

[26] F. Lavaee, M. Yousefi, P. Haddadi, Comparison of the fungicidal efficacy of photodynamic therapy with methylene blue, silver nanoparticle, and their conjugation on oral Candida isolates using cell viability assay, Curr. Med. Mycol. 6 (2020) 35–40. https://doi.org/10.18502/cmm.6.4.5332.

[27] B. Le Ouay, F. Stellacci, Antibacterial activity of silver nanoparticles: A surface science insight, Nano Today. 10 (2015) 339–354. https://doi.org/https://doi.org/10.1016/j.nantod.2015.04.002.

[28] T. de Oliveira-Silva, L.H. Alvarenga, C. Lima-Leal, B. Godoy-Miranda, P. Carribeiro, L.C. Suzuki, M. Simões Ribeiro, I. Tiemy Kato, C. Pavani, R.A. Prates, Effect of photodynamic antimicrobial chemotherapy on Candida albicans in the presence of glucose, Photodiagnosis Photodyn. Ther. 27 (2019) 54–58. https://doi.org/10.1016/j.pdpdt.2019.05.032.